Engineering Fracture Mechanics 77 (2010) 1577–1603

Contents lists available at ScienceDirect

Engineering Fracture Mechanics

journal homepage: www.elsevier.com/locate/engfracmech

Computational applications of a coupled plasticity-damage constitutive model for simulating plain concrete fracture

Rashid K. Abu Al-Rub *, Sun-Myung Kim

Zachry Department of Civil Engineering, Texas A&M University, College Station, TX 77843, USA

ARTICLE INFO

Article history:
Received 30 December 2009
Received in revised form 26 March 2010
Accepted 9 April 2010
Available online 14 April 2010

Keywords:
Damage mechanics
Anisotropic damage
Concrete fracture
Finite element
Tensile damage
Compressive damage

ABSTRACT

A coupled plasticity-damage model for plain concrete is presented in this paper. Based on continuum damage mechanics (CDM), an isotropic and anisotropic damage model coupled with a plasticity model is proposed in order to effectively predict and simulate plain concrete fracture. Two different damage evolution laws for both tension and compression are formulated for a more accurate prediction of the plain concrete behavior. In order to derive the constitutive equations and for the easiness in the numerical implementation, in the CDM framework the strain equivalence hypothesis is adopted such that the strain in the effective (undamaged) configuration is equivalent to the strain in the nominal (damaged) configuration. The proposed constitutive model has been shown to satisfy the thermodynamics requirements. Detailed numerical algorithms are developed for the finite element implementation of the proposed coupled plasticity-damage model. The numerical algorithm is coded using the user subroutine UMAT and then implemented in the commercial finite element analysis program Abaqus. Special emphasis is placed on identifying the plasticity and damage model material parameters from loading–unloading uniaxial test results. The overall performance of the proposed model is verified by comparing the model predictions to various experimental data, such as monotonic uniaxial tension and compression tests, monotonic biaxial compression test, loading–unloading uniaxial tensile and compressive tests, and mixed-mode fracture tests.

1. Introduction

The main motivation of this study is to develop a consistent approach using continuum damage mechanics and plasticity theory for the numerical simulation of degradation and failure of concrete structures. Concrete is a widely used material in numerous civil engineering structures due to the capability to be cast in site and the flexibility in different shapes. Although concrete material has longer history than other construction materials, the accurate modeling of its mechanical behavior under complex loading paths still represents a challenging task, especially when the prediction of failure is of interest. In order to predict precisely the fracture of concrete members and structures, it is crucial to develop a robust constitutive and computational model that can effectively describe the micro-crack nucleation and growth in plain concrete that lead to stiffness degradation of concrete structural elements and irreversible (plastic) deformations. Therefore, the objective of this paper is to describe such a computational model.

The common theories that have been used for the description of concrete constitutive behavior are plasticity, continuum damage mechanics, fracture mechanics, elastic-damage, and combined plasticity and damage mechanics. Plasticity

* Corresponding author. Tel.: +1 979 862 6603; fax: +1 979 845 6554.
E-mail address: rabualrub@civil.tamu.edu (R.K. Abu Al-Rub).

0013-7944/$ - see front matter © 2010 Elsevier Ltd. All rights reserved.
doi:10.1016/j.engfracmech.2010.04.007

theory has been used successfully in modeling the behavior of metals where the dominant mode of internal rearrangement is the slip process. Although the mathematical theory of plasticity is thoroughly established and some of these works were far superior to elastic approaches, these works failed to address the degradation of the material stiffness due to micro-cracking (e.g. [7,10,11,19,21,22,26,38,52,57,58,66,74,80]). On the other hand, continuum damage mechanics (CDM) (e.g. [35,45–47]) has also been used alone with elasticity to model the material nonlinear behavior of concrete. However, several facets of concrete behavior, such as irreversible deformations and inelastic volumetric expansion in compression cannot be described by this approach (e.g. [40,41,48,49,51,60,64,69,70]). Therefore, since both micro-cracking and irreversible deformations are contributing to the nonlinear response of concrete, a constitutive model should address equally the two physically distinct modes of irreversible changes in order to simulate the concrete nonlinear behavior properly up to fracture.

Combinations of plasticity and damage are usually based on isotropic hardening combined with either isotropic (scalar) or anisotropic (tensor) damage variables. One type of combination relies on stress-based plasticity formulated in the effective (undamaged) space (e.g. [13,16,23,29–31,33,34,44,53,65,69,70,79,81,82]), where the effective stress is defined as the average micro-scale stress acting on the undamaged material between micro-defects. Another type is based on stress-based plasticity in the nominal (damaged) stress space (e.g. [5,6,9,28,37,50,59]), where the nominal stress is defined as the macro-scale stress acting on both damaged and undamaged material. However, it is shown by Abu Al-Rub and Voyiadjis [2] that coupled plastic-damage models formulated in the effective space are numerically more stable and attractive. On the other hand, for better characterization of the concrete damage behavior, anisotropic damage effects, i.e. different micro-cracking in different directions, should be characterized [34]. However, anisotropic damage in concrete is complex and the coupling with plasticity and the application to structural analysis is not straightforward (e.g. [8,13,27,33,34,53,74,76,82]), and, therefore, it has been avoided by many authors.

In this paper, comprehensive and unified integration of various aspects of modeling concrete material is presented. The following aspects are integrated in this model: (1) a coupled anisotropic damage and plasticity constitutive model that predicts the concrete's distinct behavior in tension and compression is formulated within the basic principles of thermodynamics, (2) the framework of continuum damage mechanics is modified in order to include quadratic isotropic and anisotropic variation of the effective stress in terms of the nominal stress, (3) two different damage evolution laws for both tension and compression are proposed and examined for a more accurate prediction of concrete behavior after the initiation of damage, (4) pertinent computational aspects concerning the algorithmic aspects and numerical implementation of the proposed constitutive model in the well-known finite element code Abaqus [1] are presented, (5) special emphasis is placed on the development of a simple procedure for the identification of damage material parameter for which very little details have been reported in the literature to address this important issue. Generally, the choice of the damage model parameters appears to be arbitrary. (6) Furthermore, in order to validate and demonstrate the capability of the proposed model and calibrated material constants, numerical results obtained with the proposed model are compared with experimental results: monotonic uniaxial tension and compression, uniaxial loading–unloading tension and compression, monotonic biaxial compression, and mixed mode fracture of double-edge-notched concrete specimen.

It is noteworthy that the softening behavior (i.e. post-peak behavior) of concrete materials due to damage evolution will lead to finite element method results that are mesh-dependent due to absence of a material length scale in the proposed local constitutive equations. In order to alleviate this mesh-dependency, the proposed constitutive model can be modified be introducing explicitly or implicitly material length scales in the constitutive equations. There are several method to achieve this; namely, the integral nonlocal theory (e.g. [18,25,32,55,62]), the gradient-dependent theory (e.g. [15,20]), and cohesive zone models (e.g. [61]). Abu Al-Rub and Voyiadjis [4] have recently extended Cicekli et al. [13] coupled plasticity-damage model for concrete materials by making the damage evolution laws nonlocal by using the gradient-dependent damage theory. In this paper, emphasis is placed on the local constitutive model and inclusion of nonlocal effects is beyond the scope of this paper.

The paper is organized as follows. A coupled plasticity-damage model which incorporates either isotropic or anisotropic damage variable is presented in Section 2. In order to illustrate the consistency of the formulation, in Section 3 the evolution laws are shown to satisfy the laws of thermodynamics. Detailed numerical algorithms for integrating the plasticity and damage constitutive equations and their implementation in the finite element code Abaqus are presented in Section 4. In Section 5, in order to demonstrate the capability of the proposed constitutive model, the predictions of several numerical examples as compared to experimental results are presented. The calibration of the model parameters associated with the plasticity and damage evolution equations is also presented. It is shown that these plasticity and damage parameters should be identified from stress–strain diagrams with loading–unloading curves.

2. Plastic-damage model for plain concrete

The coupled plasticity-damage model formulated recently by Cicekli et al [13] for plain concrete is recalled and modified in this section. In order to predict the plastic behavior of plain concrete, the Lubliner yield criterion [44,50] expressed in the effective (undamaged) configuration is adopted. Moreover, the non-associative plasticity flow rule based on the Drucker–Prager potential and two distinct damage evolution surfaces; tensile and compressive damage surfaces are included in the model.

Damage in materials can be represented in many forms such as specific void and crack surfaces, specific crack and void volumes, the spacing between cracks or voids. In this paper, however, the physical interpretation of the damage variable is introduced as the specific damage surface area.

2.1. Isotropic damage model

The definition of the damage variable φ in one-dimension proposed by Kachanov [35] is adopted and recalled here for completeness. Consider a uniform bar subjected to a uniaxial tensile load T as shown in Fig. 1a. The whole cross-sectional area of the bar in the damaged configuration is A and the total damage area A^D is an area formed by both voids and cracks due to damage in the bar [36,76]. Furthermore, a fictitious undamaged (effective) configuration of the bar as shown in Fig. 1b is considered in order to use the principles of continuum damage mechanics. In this effective configuration all types of damage, including both voids and cracks, are removed from the bar. The effective stressed cross-sectional area of the bar in this configuration is denoted by $\overline{A}$. The damage density φ is defined by the ratio of the total damaged area to whole cross-sectional area of the bar and is expressed simply as follows:

$$\varphi = \frac{A - \overline{A}}{A} = \frac{A^D}{A} \tag{1}$$

The damage density φ can be varied from 0 to 1. The damage density is equal to zero means that the material is undamaged and one means that the material is fully damaged.

Because the bar in both the damaged and the effective configuration are subjected to the same tensile force T, the following expression for the uniaxial stress σ [35,63] of damaged configuration is derived considering the relation between the applied force and the resultant stress for both configurations:

$$\sigma = (1 - \varphi)\bar{\sigma} \tag{2}$$

Similarly, the relation between the nominal stress tensor σ_{ij} and the effective stress tensor $\bar{\sigma}_{ij}$ for the isotropic damage (i.e. scalar damage variable) can be written as follows:

$$\sigma_{ij} = (1 - \varphi)\bar{\sigma}_{ij} \tag{3}$$

Therefore, in the continuum damage mechanics framework, the effective stress means the average micro-level stress acting in the undamaged (intact) material between defects and is defined as the force divided by the undamaged part of the area, while the nominal stress means the macro-level stress and is defined as the force divided by the total area.

The above definition has been modified by Voyiadjis et al. [78] in order to include non-local damage effects in order to eliminate the mesh-sensitivity problem due to damage localization, such that:

$$\sigma_{ij} = \left(1 - \widehat{\varphi}\right)\bar{\sigma}_{ij} \quad \text{with} \quad \widehat{\varphi} = \varphi + \ell^2\nabla^2\varphi \tag{4}$$

where $\widehat{\varphi}$ is the non-local damage density, $\ell$is a material length scale parameter, and ∇^2 is the Laplacian operator. The use of Eq. (4) instead of Eq. (3) is the main focus of the work by Abu Al-Rub and Voyiadjis [4] and is beyond the scope of current study. The main focus of the current work is on the development, calibration, numerical implementation, and application of a robust constitutive plastic-damage model for concrete materials.

In order to derive the transformation relations between the damaged and the hypothetical undamaged states of the material, the strain equivalence hypothesis is adopted in this paper for simplicity and ease in numerical implementation. This hypothesis states that the elastic and plastic strains in both the damaged and the effective configurations due to the applied

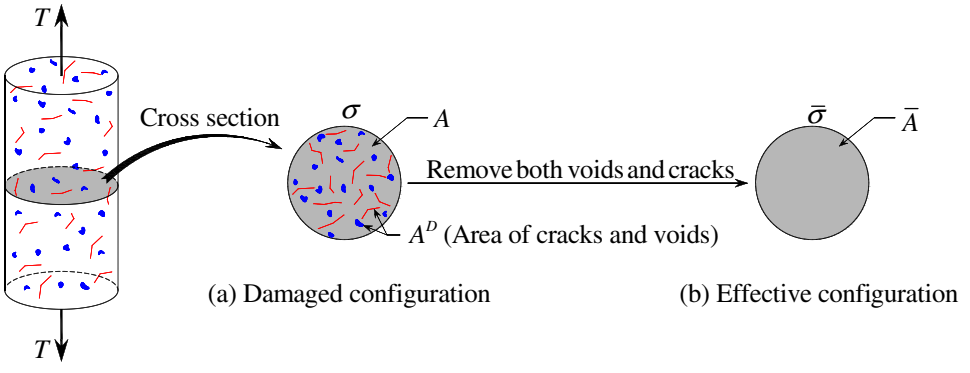

Fig. 1. A cylindrical bar subjected to uniaxial tension.

force are equivalent. Therefore, the total strain tensor ε_{ij} is set equal to the corresponding effective strain tensor $\bar{\varepsilon}_{ij}$ (i.e. $\varepsilon_{ij} = \bar{\varepsilon}_{ij}$), which can be decomposed into an elastic strain $\varepsilon^e_{ij}(= \bar{\varepsilon}^e_{ij})$ and a plastic strain $\varepsilon^p_{ij}(= \bar{\varepsilon}^p_{ij})$, such that:

$$\varepsilon_{ij} = \varepsilon^e_{ij} + \varepsilon^p_{ij} = \bar{\varepsilon}^e_{ij} + \bar{\varepsilon}^p_{ij} = \bar{\varepsilon}_{ij} \tag{5}$$

The plastic strain in Eq. (5) incorporates all types of irreversible deformations whether they are due to tensile microcracking, breaking of internal bonds during shear loading, and/or compressive consolidation during the collapse of the micro-porous structure of the cement matrix.

Applying the hypothesis of the strain equivalence, the relation between the damaged elasticity tensor E_{ijkl} and the effective (undamaged) elasticity tensor $\bar{E}_{ijkl}$ can be expressed using the generalized Hooke's law as follows:

$$E_{ijkl} = (1 - \varphi)\bar{E}_{ijkl} \tag{6}$$

This relation states that the damaged stiffness is decreased linearly as the damage density φ increases. The concept of the isotropic damage model applying the hypothesis of the strain equivalence is very simple and has given a lot of inspirations to researchers. This damage model, however, is not fully capable of predicting the nonlinearity of the damaged stiffness degradation observed from the experiments due to the increase of the damage density [13].

2.2. Modified isotropic damage model

The motivation of the modified isotropic damage model is that the damaged stiffness varies nonlinearly with the damage density as argued by Cicekli et al. [13]. Therefore, in order to predict the nonlinear degradation of the damaged stiffness due to the increase of the damage density, a nonlinear relationship between the nominal and the effective stress tensor is assumed such that:

$$\sigma_{ij} = (1 - \varphi)^{\alpha}\bar{\sigma}_{ij} \tag{7}$$

where α is a material constant. In the following development $\alpha = 2$ will be assumed such that

$$\sigma_{ij} = (1 - \varphi)^2\bar{\sigma}_{ij} \tag{8}$$

By applying the strain equivalence hypothesis, the damaged elasticity tensor E_{ijkl} can be expressed as follows:

$$E_{ijkl} = (1 - \varphi)^2\bar{E}_{ijkl} \tag{9}$$

One can also use the strain energy equivalence hypothesis [76] to obtain a nonlinear relationship between stiffness and the damage density as in Eq. (9); however, this will complicate the constitutive models and the numerical implementation. This issue has been discussed thoroughly by Abu Al-Rub and Voyiadjis [2].

Since concrete has a distinct behavior in tension and compression and, therefore, in order to adequately characterize the damage in concrete due to tensile, compressive, and/or cyclic loadings, the Cauchy stress tensor (in the nominal or effective configurations) is decomposed into positive and negative parts using the spectral decomposition technique [42,69,70]. Hereafter, the superscripts "+" and "−" designate, respectively, tensile and compressive entities. Therefore, the nominal stress tensor σ_{ij} and the effective stress tensor $\bar{\sigma}_{ij}$ can be decomposed as follows:

$$\sigma_{ij} = \sigma^+_{ij} + \sigma^-_{ij}, \quad \bar{\sigma}_{ij} = \bar{\sigma}^+_{ij} + \bar{\sigma}^-_{ij} \tag{10}$$

where σ^+_{ij} and $\bar{\sigma}^+_{ij}$ are the tensile parts whereas σ^-_{ij} and $\bar{\sigma}^-_{ij}$ are the compressive parts of the stress tensor.

Using fourth-order tensile and compressive projection tensors P^+_{ijkl} and P^-_{ijkl}, the nominal tensile and compressive stress tensors $\bar{\sigma}^+_{ij}$ and $\bar{\sigma}^-_{ij}$ can be related to $\bar{\sigma}_{ij}$ by

$$\bar{\sigma}^+_{kl} = P^+_{klpq}\bar{\sigma}_{pq}, \quad \bar{\sigma}^-_{kl} = P^-_{klpq}\bar{\sigma}_{pq} \tag{11}$$

where the projection tensors are defined as follows:

$$P^+_{ijpq} = \sum_{k=1}^{3} H(\hat{\bar{\sigma}}^{(k)})n^{(k)}_i n^{(k)}_j n^{(k)}_p n^{(k)}_q, \quad P^-_{ijpq} = I_{ijpq} - P^+_{ijpq} \tag{12}$$

where $H(\hat{\bar{\sigma}}^{(k)})$ denotes the Heaviside step function computed at kth principal stress $\hat{\sigma}^{(k)}$ of σ_{ij} and $n^{(k)}_i$ is the kth corresponding unit principal directions. In the subsequent development, the superimposed hat designates a principal value.

Based on the decomposition in Eq. (10), the expression in Eq. (8) can be assumed to be valid for both tension and compression, such that:

$$\sigma^+_{ij} = (1 - \varphi^+)^2\bar{\sigma}^+_{ij}, \quad \sigma^-_{ij} = (1 - \varphi^-)^2\bar{\sigma}^-_{ij} \tag{13}$$

where φ^+ and φ^- are the tensile and compressive damage densities, respectively. Therefore, by substituting Eq. (13) into Eq. $(10)_1$, σ_{ij} can be expressed as follows:

$$\sigma_{ij} = (1 - \varphi^+)^2\bar{\sigma}^+_{ij} + (1 - \varphi^-)^2\bar{\sigma}^-_{ij} \tag{14}$$

In the above expression the explicit decoupling between the tensile and compressive damage densities is assumed, but they are coupled implicitly such that degradation in the tensile strength will cause further degradation in the compressive strength and vice versa.

By substituting Eq. (11) into Eq. (14), one can write the following relation between σ_{ij} and $\bar{\sigma}_{ij}$ in terms of φ^+ and φ^-, such that:

$$\sigma_{ij} = \left[(1-\varphi^+)^2 P^+_{ijkl} + (1-\varphi^-)^2 P^-_{ijkl}\right]\bar{\sigma}_{kl} \tag{15}$$

2.3. Extension to anisotropic damage

Anisotropic damage is considered in this study for a more reliable representation of concrete damage behavior. Isotropic damage assumes that the strength and stiffness of the concrete material is degraded equally in different directions upon damage evolution which is not realistic. Therefore, in order to include damage-induced anisotropy (i.e. different degradation in different directions), the relation between σ_{ij} and $\bar{\sigma}_{ij}$ can be expressed as follows (e.g. [17,54,76]):

$$\sigma_{ij} = M_{ijkl}\bar{\sigma}_{kl} \tag{16}$$

where M_{ijkl} is the fourth-order damage-effect tensor that is used to make the stress tensor symmetrical. There are several definitions for the tensor M_{ijkl} [75]; however, a different definition is presented in this paper as follows:

$$M_{ijkl} = \frac{1}{2}\left[(\delta_{im}-\varphi_{im})(\delta_{jm}-\varphi_{jm})\delta_{kl} + \delta_{ij}(\delta_{km}-\varphi_{km})(\delta_{lm}-\varphi_{lm})\right] \tag{17}$$

where δ_{ij} is the Kronecker delta and φ_{ij} is a second-order damage tensor.

Using the generalized Hooke's law, σ_{ij} and $\bar{\sigma}_{ij}$ are given as follows:

$$\sigma_{ij} = E_{ijkl}\varepsilon^e_{kl}, \quad \bar{\sigma}_{ij} = \overline{E}_{ijkl}\varepsilon^e_{kl} \tag{18}$$

For isotropic linear-elastic material, $\overline{E}_{ijkl}$ is given by

$$\overline{E}_{ijkl} = 2\overline{G}\delta_{ik}\delta_{jl} + \left(\overline{K} - \frac{2}{3}\overline{G}\right)\delta_{ij}\delta_{kl} \tag{19}$$

where $\overline{G} = \overline{E}/2(1+\bar{\nu})$ and $\overline{K} = \overline{E}/3(1-2\bar{\nu})$ are the effective shear and bulk moduli, respectively, with $\overline{E}$ being the Young's modulus and $\bar{\nu}$ is the Poisson's ratio which are obtained from the stress–strain diagram in the effective configuration.

From the Eq. (18) and since the strain equivalence hypothesis is adopted, the elastic strain tensor ε^e_{kl} can be expressed as follows:

$$\varepsilon^e_{ij} = E^{-1}_{ijkl}\sigma_{kl} = \overline{E}^{-1}_{ijkl}\bar{\sigma}_{kl} \tag{20}$$

where E^{-1}_{ijkl} is the inverse (or compliance tensor) of the fourth-order damaged elastic tensor E_{ijkl}, which is a function of the damage variable φ_{ij}.

By substituting Eq. (16) into Eq. (18) or Eq. (20), one can express the damaged elasticity tensor E_{ijkl} in terms of the corresponding undamaged elasticity tensor $\overline{E}_{ijkl}$ by the following relation:

$$E_{ijkl} = M_{ijmn}\overline{E}_{mnkl} \tag{21}$$

Based on Eq. (10), the expression in Eq. (16) can be rewritten with decoupled damage evolution in tension and compression, such that:

$$\sigma^+_{ij} = M^+_{ijkl}\bar{\sigma}^+_{kl}, \quad \sigma^-_{ij} = M^-_{ijkl}\bar{\sigma}^-_{kl} \tag{22}$$

where M^+_{ijkl} is the tensile damage-effect tensor and M^-_{ijkl} is the corresponding compressive damage effect-tensor which can be expressed using Eq. (17) in a decoupled form as a function of the tensile and compressive damage variables, φ^+_{ij} and φ^-_{ij}, respectively, as follows:

$$\begin{aligned} M^+_{ijkl} &= \frac{1}{2}\left[(\delta_{im}-\varphi^+_{im})\left(\delta_{jm}-\varphi^+_{jm}\right)\delta_{kl} + \delta_{ij}\left(\delta_{km}-\varphi^+_{km}\right)\left(\delta_{lm}-\varphi^+_{lm}\right)\right] \\ M^-_{ijkl} &= \frac{1}{2}\left[(\delta_{im}-\varphi^-_{im})\left(\delta_{jm}-\varphi^-_{jm}\right)\delta_{kl} + \delta_{ij}\left(\delta_{km}-\varphi^-_{km}\right)\left(\delta_{lm}-\varphi^-_{lm}\right)\right] \end{aligned} \tag{23}$$

Now, by substituting Eq. (22) into Eq. $(10)_1$, one can express $\bar{\sigma}_{ij}$ as follows:

$$\bar{\sigma}_{ij} = \left(M^+_{ijkl}\right)^{-1}\sigma^+_{kl} + \left(M^-_{ijkl}\right)^{-1}\sigma^-_{kl} \tag{24}$$

Similarly, σ_{ij} can be expressed as follows:

$$\sigma_{ij} = M^+_{ijkl}\bar{\sigma}^+_{kl} + M^-_{ijkl}\bar{\sigma}^-_{kl} \tag{25}$$

By substituting Eq. (11) into Eq. (24) and comparing the result with Eq. (16), the following relation for the damage-effect tensor M_{ijkl} can be obtained, such that:

$$M_{ijpq} = M^{+}_{ijkl}P^{+}_{klpq} + M^{-}_{ijkl}P^{-}_{klpq} \tag{26}$$

Using Eq. $(12)_2$, the above expression can be rewritten as:

$$M_{ijpq} = \left[M^{+}_{ijkl} - M^{-}_{ijkl}\right]P^{+}_{klpq} + M^{-}_{ijpq} \tag{27}$$

One should notice the following:

$$M_{ijkl} \neq M^{+}_{ijkl} + M^{-}_{ijkl} \tag{28}$$

or

$$\varphi_{ij} \neq \varphi^{+}_{ij} + \varphi^{-}_{ij} \tag{29}$$

It is also noteworthy that the relation in Eq. (27) enhances a coupling between tensile and compressive damage through the fourth-order projection tensor P^{+}_{ijkl}. Therefore, for isotropic damage Eq. (15) gives the following expression for the fourth-order damage-effect tensor:

$$M_{ijkl} = (1-\varphi^{+})^2P^{+}_{ijkl} + (1-\varphi^{-})^2P^{-}_{ijkl} \tag{30}$$

From the above expression, adopting the decomposition of the scalar damage variable φ into a positive φ^{+} part and a negative φ^{-} part still enhances a damage anisotropy through the spectral decomposition tensors P^{+}_{ijkl} and P^{-}_{ijkl}. However, this anisotropy is weak when compared to the anisotropic damage effect tensor presented in Eq. (27).

2.4. Plasticity yield surface

Concrete materials exhibit plastic (irreversible) deformation upon unloading which implies that an elastic-damage model is not sufficient to model the concrete behavior even under tensile loading conditions. Therefore, an elasto-plastic-damage model should be developed. Thus, a plasticity yield surface and plasticity flow rules need to be developed. Furthermore, since concrete material behaves differently in tension and compression, the yield criterion of Lubliner et al. [50] that accounts for both tension and compression plasticity is adopted in this paper. However, since the stress state in the intact material is the one which drives the plasticity evolution, this yield criterion is expressed in the effective (undamaged) configuration as follows:

$$f = \sqrt{3\bar{J}_2} + \alpha\bar{I}_1 + \beta(\varepsilon^{+}_{eq},\varepsilon^{-}_{eq})\mathrm{H}(\hat{\bar{\sigma}}_{\max})\hat{\bar{\sigma}}_{\max} - (1-\alpha)c^{-}(\varepsilon^{-}_{eq}) \leqslant 0 \tag{31}$$

where $\bar{J}_2 = \bar{s}_{ij}\bar{s}_{ij}/2$ is the second-invariant of the effective deviatoric stress tensor $\bar{s}_{ij} = \bar{\sigma}_{ij} - \bar{\sigma}_{kk}\delta_{ij}/3$, $\bar{I}_1 = \bar{\sigma}_{kk}$ is the first-invariant of the effective Cauchy stress tensor $\bar{\sigma}_{ij}$, $\hat{\bar{\sigma}}_{\max}$ is the maximum principal effective stress, $\mathrm{H}(\hat{\bar{\sigma}}_{\max})$ is the Heaviside step function (H=1 for $\hat{\bar{\sigma}}_{\max} > 0$ and H=0 for $\hat{\bar{\sigma}}_{\max} < 0$), and the parameters α and β are dimensionless constants which are defined as follows:

$$\alpha = \frac{(f_{b0}/f^{-}_{0}) - 1}{2(f_{b0}/f^{-}_{0}) - 1}, \quad \beta = (1-\alpha)\frac{c^{-}(\varepsilon^{-}_{eq})}{c^{+}(\varepsilon^{+}_{eq})} - (1+\alpha) \tag{32}$$

with f_{b0} and f^{-}_{0} being the initial equi-biaxial and uniaxial compressive yield strengths, respectively.

Experimental values for f_{b0}/f^{-}_{0} lie between 1.10 and 1.16; yielding values for α between 0.08 and 0.12. The shape of the yield surface for two values of the dilatational constant α and its comparison with the experimental results by Kupfer et al. [43] are shown in Fig. 2. As seen, when $\alpha = 0.12$, the model gives a better prediction of the experimental results, and consequently, this value is used for α in this study.

The internal plastic state variables $\varepsilon^{+}_{eq} = \int_0^t \dot{\varepsilon}^{+}_{eq}\,\mathrm{d}t$ and $\varepsilon^{-}_{eq} = \int_0^t \dot{\varepsilon}^{-}_{eq}\,\mathrm{d}t$ are the equivalent plastic strains in tension and compression, respectively, where their rates are defined as follows:

$$\dot{\varepsilon}^{+}_{eq} = r(\hat{\bar{\sigma}}_{ij})\dot{\hat{\varepsilon}}^{p}_{\max}, \quad \dot{\varepsilon}^{-}_{eq} = -(1-r(\hat{\bar{\sigma}}_{ij}))\dot{\hat{\varepsilon}}^{p}_{\min} \tag{33}$$

where $\dot{\hat{\varepsilon}}^{p}_{\max}$ and $\dot{\hat{\varepsilon}}^{p}_{\min}$ are the maximum and minimum principal values of the plastic strain rate $\dot{\varepsilon}^{p}_{ij}$ such that $\hat{\varepsilon}^{p}_{1} > \hat{\varepsilon}^{p}_{2} > \hat{\varepsilon}^{p}_{3}$ with $\hat{\varepsilon}^{p}_{\max} = \hat{\varepsilon}^{p}_{1}$ and $\hat{\varepsilon}^{p}_{\min} = \hat{\varepsilon}^{p}_{3}$. Note that the superscript + or − designates a tensile or compressive quantity, $(\hat{\bullet})$ designates the principle value of $(\bullet)$, and the subscripts *eq*, min, and max are not indicial indices. The dimensionless parameter $r(\hat{\bar{\sigma}}_{ij})$ is a weight factor for tension or compression depending on the values of the principal stresses and is defined as follows:

$$r(\hat{\bar{\sigma}}_{ij}) = \frac{\sum_{k=1}^{3}\left\langle\hat{\bar{\sigma}}_k\right\rangle}{\sum_{k=1}^{3}\left|\hat{\bar{\sigma}}_k\right|} \tag{34}$$

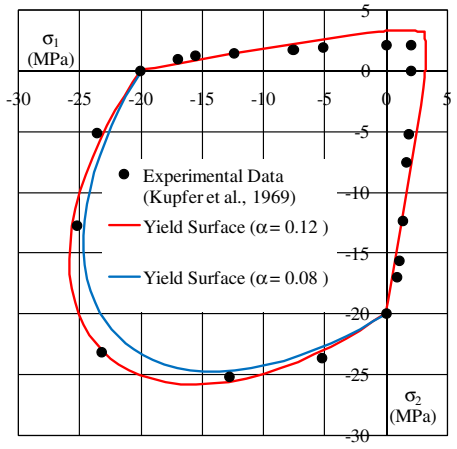

Fig. 2. Lubliner plasticity yielding surface for different values of α. Comparison with experimental results by Kupfer et al. [43].

where $\langle\rangle$ is the McAuley bracket presented as $\langle x\rangle = \frac{1}{2}(|x| + x)$. Note that $r(\hat{\bar{\sigma}}_{ij}) = r(\hat{\sigma}_{ij})$. Moreover, depending on the value of $r(\hat{\bar{\sigma}}_{ij})$: (a) if the loading is pure uniaxial tension $\hat{\bar{\sigma}}_k \geqslant 0$, then $r(\hat{\bar{\sigma}}_{ij}) = 1$, and (b) if the loading is pure uniaxial compression $\hat{\bar{\sigma}}_k \leqslant 0$, then $r(\hat{\bar{\sigma}}_{ij}) = 0$.

In the last term of Eq. (31), the isotropic hardening function c^- represents the material cohesion in uniaxial compression. Since the concrete behavior in compression is more of a ductile behavior as compared to its corresponding brittle behavior in tension, the evolution of the compressive and tensile isotropic hardening functions c^- and c^+ are defined by the following exponential and linear hardening laws, respectively:

$$c^- = f_0^- + Q^-\left[1 - \exp(-b^-\varepsilon_{eq}^-)\right], \quad c^+ = f_0^+ + h^+\varepsilon_{eq}^+ \tag{35}$$

where f_0^- and f_0^+ are the initial yield stresses in compression and tension (i.e. when nonlinear behavior starts), respectively. The parameters Q^-, b^-, and h^+ are material constants, which are obtained in the effective configuration of the uniaxial stress–strain diagram.

For realistic modeling of the volumetric expansion under compression of concrete, a non-associative plasticity flow rule should be used. This can be done by writing the evolution of the plastic strain tensor $\dot{\varepsilon}_{ij}^p$, in terms of a plastic potential F^p that is not equal to the plastic yield function f, such that:

$$\dot{\varepsilon}_{ij}^p = \dot{\lambda}^p \frac{\partial F^p}{\partial \bar{\sigma}_{ij}} \tag{36}$$

where $\dot{\lambda}^p$ is the plastic multiplier, which can be obtained using the standard plasticity consistency condition, $\dot{f} = 0$, such that:

$$f \leqslant 0, \dot{\lambda}^p \geqslant 0, \quad \dot{\lambda}^p f = 0, \quad \dot{\lambda}^p \dot{f} = 0 \tag{37}$$

The plastic potential F^p can be expressed in terms of the Drucker–Prager function as:

$$F^p = \sqrt{3\bar{J}_2} + \alpha^p \bar{I}_1 \tag{38}$$

where α^p is the dilation material constant. Then the plastic flow direction $\partial F^p/\partial\bar{\sigma}_{ij}$ in Eq. (36) is given by

$$\frac{\partial F^p}{\partial \bar{\sigma}_{ij}} = \frac{3}{2}\frac{\bar{s}_{ij}}{\sqrt{3\bar{J}_2}} + \alpha^p \delta_{ij} \tag{39}$$

2.5. Tensile and compressive damage surfaces

The following damage growth function which is proposed by Chow and Wang [12] and used by many others (see e.g. [2,3,77,78], and the references quoted therein) is adopted in this study. However, this function is generalized in Cicekli et al. [13] in order to incorporate both tensile and compressive damage separately, such that:

$$g^\pm = \sqrt{\frac{1}{2}Y_{ij}^\pm L_{ijkl}^\pm Y_{kl}^\pm} - K^\pm(\varphi_{eq}^\pm) \leqslant 0 \tag{40}$$

where $K^\pm$ is the tensile or compressive damage isotropic hardening function such that $K^\pm = K_0^\pm$ when there is no damage, where $K_0^\pm$ is the tensile or compressive initial damage parameter (i.e. damage threshold) which is interpreted as the area under the linear portion of the stress–strain diagram, and $L_{ijkl}^\pm$ is a fourth-order symmetric tensor. In what follows, $L_{ijkl}^\pm$ is taken as the fourth-order identity tensor I_{ijkl} in order to simplify the anisotropic damage formulation.

It is also noteworthy that one can assume that when concrete is under tensile loading, the tensile yielding of the material is almost coincide with the damage initiation. Therefore, the tensile yield strength f_0^+ and the tensile damage threshold K_0^+ have almost the same value. When concrete is under compressive loading, however, the compressive damage is initiated later than the compressive yielding of the material. Therefore, the compressive damage threshold K_0^- is always greater than the compressive yield strength f_0^-.

The damage driving force $Y_{ij}^{\pm}$ is interpreted as the energy release rate according to the notion of fracture mechanics as argued by Abu Al-Rub and Voyiadjis [2], where the following expression is proposed:

$$Y_{rs}^{\pm} = -\frac{1}{2}\bar{E}^{-1}_{ijab}\bar{\sigma}_{ab}\frac{\partial M_{ijpq}}{\partial \varphi_{rs}^{\pm}}\bar{\sigma}_{pq} \tag{41}$$

The rate of the equivalent damage $\dot{\varphi}_{eq}^{\pm}$ (i.e. rate of damage accumulation) is defined as:

$$\dot{\varphi}_{eq}^{\pm} = \sqrt{\dot{\varphi}_{ij}^{\pm}\dot{\varphi}_{ij}^{\pm}} \quad \text{with } \varphi_{eq}^{\pm} = \int_0^t \dot{\varphi}_{eq}^{\pm}\,\mathrm{d}t \tag{42}$$

The evolution equation for $\dot{\varphi}_{ij}^{\pm}$ is defined by:

$$\dot{\varphi}_{ij}^{\pm} = \dot{\lambda}_d^{\pm}\frac{\partial g^{\pm}}{\partial Y_{ij}^{\pm}} \tag{43}$$

where $\dot{\lambda}_d^{\pm}$ is the damage multiplier such that one can easily show from Eqs. (40)–(43) that $\dot{\lambda}_d^{\pm} = \dot{\varphi}^{\pm}$. This multiplier can be obtained from the following damage consistency conditions:

$$g^{\pm} \leqslant 0, \quad \dot{\lambda}_d^{\pm} g^{\pm} = 0, \quad \text{and } \dot{g}^{\pm}\left\{\begin{array}{l} < 0 \Rightarrow \dot{\lambda}_d^{\pm} = 0 \\ = 0 \Rightarrow \dot{\lambda}_d^{\pm} = 0 \\ = 0 \Rightarrow \dot{\lambda}_d^{\pm} > 0 \end{array}\right\} \Longleftrightarrow \left\{\begin{array}{l} \text{effective (undamaged state)} \\ \text{damage initiation} \\ \text{damage growth} \end{array}\right. \tag{44}$$

2.6. Tensile and compressive damage evolution laws

In this paper, two damage evolution laws, an exponential law and a power law, for both tensile and compressive loading cases are proposed and tested to see which one is more suitable than the other in predicting the damage behavior in concrete when compared to experimental data.

2.6.1. Exponential damage evolution law

The following exponential tensile and compressive damage evolution laws are proposed for $\varphi_{eq}^{\pm}$ in Eq. (42):

$$\varphi_{eq}^{+} = 1 - \left(\frac{K_0^+}{K^+}\right)\exp\left[B^+\left(1 - \frac{K^+}{K_0^+}\right)\right] \tag{45}$$

$$\varphi_{eq}^{-} = 1 - \exp\left[B^-\left(1 - \frac{K^-}{K_0^-}\right)\right] \tag{46}$$

where $B^{\pm}$ is a material constant, which is related to the tensile and compressive fracture energies, and therefore can be calibrated from the uniaxial tensile and compressive stress–strain diagrams. Both exponential damage evolution laws have similar form, however, the term K_0^+/K^+, the ratio of the tensile damage threshold to the tensile damage hardening function, is multiplied to the tensile damage evolution law in order to control the tensile damage evolution rate. The main advantage of the exponential damage evolution law is that there is only one material constant in each law, $B^{\pm}$, which needs to be identified from experimental data. The above expressions are to a great extent similar to those proposed by Mazars and Pijaudier-Cabot [51].

In the case of using the exponential damage evolution law, the evolution of the tensile and compressive damage isotropic hardening functions $\dot{K}^+$ and $\dot{K}^-$ in Eq. (40) can be derived by taking time derivative of Eqs. (45) and (46) as follows:

$$\dot{K}^{+} = \frac{K^+}{B^+ + \frac{K_0^+}{K^+}}\exp\left[-B^+\left(1 - \frac{K^+}{K_0^+}\right)\right]\dot{\varphi}_{eq}^{+} \tag{47}$$

$$\dot{K}^{-} = \frac{K_0^-}{B^-}\exp\left[-B^-\left(1 - \frac{K^-}{K_0^-}\right)\right]\dot{\varphi}_{eq}^{-} \tag{48}$$

The above evolution equations are useful in the development of numerical algorithms as is seen later in this paper.

2.6.2. Power damage evolution law

The following power tensile and compressive damage evolution laws are proposed in order to improve the capability of the damage model for the prediction of the concrete behavior and to compare it to the exponential damage low which is widely used in the literature, such that:

$$\varphi_{eq}^{+} = B^{+}\left(\frac{K_0^{+}}{K^{+}}\right)\left(\frac{K^{+}}{K_0^{+}} - 1\right)^{q^{+}} \tag{49}$$

$$\varphi_{eq}^{-} = B^{-}\left(\frac{K^{-}}{K_0^{-}} - 1\right)^{q^{-}} \tag{50}$$

where $B^{\pm}$ and $q^{\pm}$ are material constants. The expense of this proposition is that one needs to identify more material constant from experimental data as compared to the exponential damage laws. However, it will be shown in the analysis section that even setting $q^{\pm} = 1$ gives better predictions than the exponential damage laws.

Similarly, for the power damage laws, one can obtain the evolution of the damage isotropic hardening functions $\dot{K}^{+}$ and $\dot{K}^{-}$ by taking the time derivative of Eqs. (49) and (50) as follows:

$$\dot{K}^{+} = \frac{K^{+}}{B^{+}\left(q^{+}K_0^{+} - 1 + \frac{K_0^{+}}{K^{+}}\right)}\left[\frac{K^{+}}{K_0^{+}} - 1\right]^{1-q^{+}}\dot{\varphi}_{eq}^{+} \tag{51}$$

$$\dot{K}^{-} = \frac{K_0^{-}}{B^{-}q^{-}}\left[\frac{K^{-}}{K_0^{-}} - 1\right]^{1-q^{-}}\dot{\varphi}_{eq}^{-} \tag{52}$$

It is noted that the tensile and compressive exponential and power damage evolution laws in Eqs. (45) and (46) and Eqs. (49) and (50) obey the fundamental principle that the damage is not initiated until the damage hardening function $K^{\pm}$ is greater than the damage threshold $K_0^{\pm}$.

For the sake of completeness, in Appendix A the thermodynamic admissibility of the presented plastic-damage model in the previous sections is checked by following the internal state variable procedure of Coleman and Gurtin [14]. The constitutive equations are derived from the second law of thermodynamics, the expression of the Helmholtz free energy density, the additive decomposition of the total strain rate into elastic and plastic components, the Clausius-Duhem inequality, and the maximum dissipation principle.

3. Numerical implementation

In this section, the time descretization and numerical integration procedures for the presented elasto-plastic-damage model are presented. The evolutions of the plastic and damage internal state variables can be obtained if the Lagrangian multipliers $\dot{\lambda}^{p}$ and $\dot{\lambda}_{d}^{\pm}$ are computed. Therefore, the plasticity and damage consistency conditions, Eqs. (37) and (44), are used for computing both $\dot{\lambda}^{p}$ and $\dot{\lambda}_{d}^{\pm}$. This is shown in the subsequent developments. Then, at the beginning of the step, by applying the given strain increment $\Delta\varepsilon_{ij} = \varepsilon_{ij}^{(n+1)} - \varepsilon_{ij}^{(n)}$ and knowing the values of the stress and internal variables from the previous step, $(\cdot)^{(n)}$, the updated values at the end of the step, $(\cdot)^{(n+1)}$, are obtained.

The implemented integration scheme is divided into two sequential steps, corresponding to the plastic and damage parts of the model. In the plastic part, the plastic strain ε_{ij}^{p} and the effective stress $\bar{\sigma}_{ij}$ at the end of the step are determined by using the classical radial return mapping algorithm [68], such that one can write from Eqs. $(18)_2$, (5), and (36) the following algorithmic step:

$$\bar{\sigma}_{ij} = \bar{\sigma}_{ij}^{tr} - \bar{E}_{ijkl}\Delta\varepsilon_{kl}^{p} = \bar{\sigma}_{ij}^{tr} - \Delta\lambda^{p}\bar{E}_{ijkl}\frac{\partial F^{p}}{\partial\bar{\sigma}_{kl}^{(n)}} \tag{53}$$

where $\bar{\sigma}_{ij}^{tr} = \bar{\sigma}_{ij}^{(n)} + \bar{E}_{ijkl}\Delta\varepsilon_{kl}$ is the trial stress tensor, which is easily evaluated from the given strain increment. Also, substituting Eqs. (19) and (39) into Eq. (53), the above equation can be rewritten as follows:

$$\bar{\sigma}_{ij} = \bar{\sigma}_{ij}^{tr} - \Delta\lambda^{p}\left[\sqrt{6}\overline{G}\frac{\bar{s}_{ij}^{(n+1)}}{\left\|\bar{s}_{ij}^{(n+1)}\right\|} + 3\overline{K}\alpha^{p}\delta_{ij}\right] \tag{54}$$

where $\|\bar{s}_{ij}\| = \sqrt{\bar{s}_{ij}\bar{s}_{ij}}$ and $\bar{s}_{ij}$ is the deviatoric component of the effective stress tensor $\bar{\sigma}_{ij}$. If the trial stress is not outside the yield surface, i.e. $f(\bar{\sigma}_{ij}^{tr}, c_c^{(n)}) \leqslant 0$, the step is elastic and one sets $\Delta\lambda^{p} = 0,\ \bar{\sigma}_{ij}^{tr} = \bar{\sigma}_{ij}^{(n+1)},\ \varepsilon_{ij}^{p(n+1)} = \varepsilon_{ij}^{p(n)},\ c^{\pm(n+1)} = c^{\pm(n)}$. However, if the trial stress is outside the yield surface, then $\bar{\sigma}_{ij}^{(n+1)},\ \varepsilon_{ij}^{p(n+1)}$, and $c^{\pm(n+1)}$ are determined by computing $\Delta\lambda^{p}$.

In the damage part, the nominal stress σ_{ij} at the end of the step is obtained from Eq. (16) by knowing the damage variables $\varphi_{ij}^{\pm}$, which can be calculated once $\Delta\lambda_{d}^{\pm}$ are computed from the damage consistency conditions in Eq. (44). Therefore, a decoupled updating algorithm is proposed in this paper where the constitutive equations are updated first in the effective configuration and then the damaged variables are calculated in terms of the effective quantities which are then used to update the constitutive equations in the damaged configuration. In fact, this is a much simpler and more stable computational algorithm as compared to sequentially updating algorithms as presented in Voyiadjis and Abu Al-Rub [73].

3.1. Computation of the plastic multiplier

From the plasticity consistency condition in Eq. (37), one can write the following relation at $n+1$ step:

$$f^{(n+1)} = f^{(n)} + \Delta f = 0 \tag{55}$$

where

$$\Delta f = \frac{\partial f}{\partial \bar{\sigma}_{ij}}\Delta\bar{\sigma}_{ij} + \frac{\partial f}{\partial \hat{\bar{\sigma}}_{\max}}\Delta\hat{\bar{\sigma}}_{\max} + \frac{\partial f}{\partial \varepsilon^{-}_{eq}}\Delta\varepsilon^{-}_{eq} + \frac{\partial f}{\partial \varepsilon^{+}_{eq}}\Delta\varepsilon^{+}_{eq} = 0 \tag{56}$$

$$\Delta\hat{\bar{\sigma}}_{\max} = \Delta\hat{\bar{\sigma}}^{tr}_{\max} - \Delta\lambda^{p}\left[\sqrt{6}\bar{G}\frac{\left(\hat{\bar{\sigma}}_{\max} - \frac{1}{3}\bar{I}_1\right)}{\|\bar{s}_{ij}\|} + 3\bar{K}\alpha_p\right] \tag{57}$$

$$\Delta\varepsilon^{+}_{eq} = r\Delta\lambda^{p}\frac{\partial F^{p}}{\partial \hat{\bar{\sigma}}_{\max}} \tag{58}$$

$$\Delta\varepsilon^{-}_{eq} = -(1-r)\Delta\lambda^{p}\frac{\partial F^{p}}{\partial \hat{\bar{\sigma}}_{\min}} \tag{59}$$

In order to go back radially to the yield surface, the following assumption is made [68]:

$$\frac{\bar{s}^{(n+1)}_{ij}}{\left\|\bar{s}^{(n+1)}_{ij}\right\|} = \frac{\bar{s}^{tr}_{ij}}{\left\|\bar{s}^{tr}_{ij}\right\|} \tag{60}$$

Substituting Eqs. (31), (38), and (57)–(59) into Eqs. (56) and (55), and then by making few algebraic manipulations, one can obtain the plastic multiplier $\Delta\lambda^{p}$ from the following expression:

$$\Delta\lambda^{p} = \frac{f^{tr}}{H} \tag{61}$$

where f^{tr} and H are given as follows:

$$f^{tr} = \sqrt{\frac{3}{2}}\left\|\bar{s}^{tr}_{ij}\right\| + \alpha\bar{I}^{tr}_1 + \beta^{tr}H(\hat{\bar{\sigma}}^{tr}_{\max})\hat{\bar{\sigma}}^{tr}_{\max} - (1-\alpha)c^{-(n)} \tag{62}$$

$$H = 3\bar{G} + 9\bar{K}\alpha_p\alpha + \beta^{tr}H\left(\hat{\bar{\sigma}}^{tr}_{\max}\right)Z + (1-r)\frac{\partial f}{\partial \varepsilon^{-tr}_{eq}}\frac{\partial F^{p}}{\partial \hat{\bar{\sigma}}^{tr}_{\min}} - r\frac{\partial f}{\partial \varepsilon^{+tr}_{eq}}\frac{\partial F^{p}}{\partial \hat{\bar{\sigma}}^{tr}_{\max}} \tag{63}$$

with

$$Z = \sqrt{6}\bar{G}\frac{\hat{\bar{\sigma}}^{tr}_{\max}}{\left\|\bar{s}^{tr}_{ij}\right\|} + 3\bar{K}\alpha_p - \sqrt{\frac{2}{3}}\bar{G}\frac{\bar{I}^{tr}_1}{\left\|\bar{s}^{tr}_{ij}\right\|} \tag{64}$$

$$\frac{\partial F^{p}}{\partial \hat{\bar{\sigma}}^{\max tr}_{\min}} = \sqrt{\frac{3}{2}}\frac{(\hat{\bar{\sigma}}^{\max tr}_{\min} - \frac{1}{3}\bar{I}^{tr}_1)}{\left\|\bar{s}^{tr}_{ij}\right\|} + \alpha_p \tag{65}$$

$$\frac{\partial f}{\partial \varepsilon^{-tr}_{eq}} = -(1-\alpha)Q^{-}b^{-}\exp(-b^{-}\varepsilon^{-}_{eq}) \tag{66}$$

$$\frac{\partial f}{\partial \varepsilon^{+tr}_{eq}} = -\langle\hat{\bar{\sigma}}^{tr}_{\max}\rangle\frac{c^{-}(1-\alpha)h^{+}}{(c^{+})^{2}} \tag{67}$$

3.2. The elasto-plastic tangent stiffness

For the effective (undamaged) configuration, the relation between the effective stress increment $\Delta\bar{\sigma}_{ij}$ and the elastic strain increment $\Delta\bar{\varepsilon}^{e}_{ij}$ can be written in the following form from Eqs. $(18)_2$ and (36), such that:

$$\Delta\bar{\sigma}_{ij} = \bar{E}_{ijkl}\Delta\bar{\varepsilon}^{e}_{kl} = \bar{E}_{ijkl}\Delta\bar{\varepsilon}_{kl} - \Delta\lambda^{p}\bar{E}_{ijkl}\frac{\partial F^{p}}{\partial\bar{\sigma}_{kl}} \tag{68}$$

By substituting Eqs. (5) and (19) into the above equation, the above expression can be rewritten as follows:

$$\Delta\bar{\sigma}_{ij} = 2\bar{G}\Delta\bar{\varepsilon}_{ij} + \left(\bar{K} - \frac{2}{3}\bar{G}\right)\Delta\bar{\varepsilon}_{kk}\delta_{ij} - \Delta\lambda^{p}\left[2\bar{G}\frac{\partial F^{p}}{\partial\bar{\sigma}_{ij}} - 3\left(\bar{K} - \frac{2}{3}\bar{G}\right)\alpha_p\delta_{ij}\right] \tag{69}$$

Furthermore, based on a spectral decomposition of the stress tensor presented in Section 2.3, Eq. (69) can be written for the increment of the effective principal stresses $\Delta\hat{\bar{\sigma}}_{ij}$ as follows:

$$\Delta\hat{\bar{\sigma}}_{ij} = 2\overline{G}l_{ri}\Delta\bar{\varepsilon}_{rs}l_{sj} + \left(\overline{K} - \frac{2}{3}\overline{G}\right)\Delta\bar{\varepsilon}_{kk}\delta_{ij} - \Delta\lambda^{p}\left[2\overline{G}\frac{\partial F^{p}}{\partial\hat{\bar{\sigma}}_{ij}} - 3\left(\overline{K} - \frac{2}{3}\overline{G}\right)\alpha_{p}\delta_{ij}\right] \tag{70}$$

where $l_{ij} = \left[n_i^{(1)}\ n_i^{(2)}\ n_i^{(3)}\right]^T$ is a second-order tensor that contains the principal directions of $\bar{\sigma}_{ij}$, where $n_i^{(1)}$, $n_i^{(2)}$, and $n_i^{(3)}$ are the eigenvectors that corresponds to $\hat{\bar{\sigma}}^{(1)} = \hat{\bar{\sigma}}_{\max}$, $\hat{\bar{\sigma}}^{(2)}$, and $\hat{\bar{\sigma}}^{(3)} = \hat{\bar{\sigma}}_{\min}$, respectively, and $[]^T$ designates the transpose. Thus, one can write from Eq. (70) the increment in the maximum principal stress $\Delta\bar{\sigma}_{\max}$ as follows:

$$\Delta\hat{\bar{\sigma}}_{\max} = 2\overline{G}n_i^{(1)}\Delta\bar{\varepsilon}_{ij}n_j^{(1)} + \left(\overline{K} - \frac{2}{3}\overline{G}\right)\Delta\bar{\varepsilon}_{kk} - \Delta\lambda^{p}\left[2\overline{G}\frac{\partial F^{p}}{\partial\hat{\bar{\sigma}}_{\max}} + 3\left(\overline{K} - \frac{2}{3}\overline{G}\right)\alpha_{p}\right] \tag{71}$$

By substituting Eqs. (69), (71) and (33) into Eq. (56) and making few algebraic manipulations, one can get the expression of the plastic multiplier $\Delta\lambda^p$ as a function of the strain rate $\Delta\bar{\varepsilon}_{ij}$ as follows:

$$\Delta\lambda^{p} = \frac{1}{H}\left\{\frac{\partial f}{\partial\bar{\sigma}_{ij}}\overline{E}_{ijkl} + 2\overline{G}\frac{\partial f}{\partial\hat{\bar{\sigma}}_{\max}}n_k^{(1)}n_l^{(1)} + \left(\overline{K} - \frac{2}{3}\overline{G}\right)\frac{\partial f}{\partial\hat{\bar{\sigma}}_{\max}}\delta_{kl}\right\}\Delta\bar{\varepsilon}_{kl} \tag{72}$$

where H is already defined in Eq. (63). Then, by substituting Eq. (72) into Eq. (68), the stress rate $\Delta\bar{\sigma}_{ij}$ can be rewritten as a function of the rate of the total strain $\Delta\bar{\varepsilon}_{ij}$ as follows:

$$\Delta\bar{\sigma}_{ij} = \overline{D}_{ijkl}\Delta\bar{\varepsilon}_{kl} \tag{73}$$

where the fourth-order tensor $\overline{D}_{ijkl}$ represents the elasto-plastic tangent stiffness in the effective configuration and is expressed as follows:

$$\overline{D}_{ijkl} = \overline{E}_{ijkl} - \frac{1}{H}\left\{\overline{E}_{mnkl}\frac{\partial f}{\partial\bar{\sigma}_{mn}} + \frac{\partial f}{\partial\hat{\bar{\sigma}}_{\max}}\left[2\overline{G}n_k^{(1)}n_l^{(1)} + \left(\overline{K} - \frac{2}{3}\overline{G}\right)\right]\delta_{kl}\right\}\overline{E}_{ijpq}\frac{\partial F^{p}}{\partial\bar{\sigma}_{pq}} \tag{74}$$

The above equation retains $\overline{D}_{ijkl} = \overline{E}_{ijkl}$ if the material is under elastic deformation or there is no plastic flow.

3.3. Computation of the tensile and compressive damage multipliers

In the following, the damage multipliers, $\dot{\lambda}_d^{\pm}$, are obtained using the consistency conditions in Eq. (44). The incremental expression for the damage consistency condition can be written as:

$$g^{\pm(n+1)} = g^{\pm(n)} + \Delta g^{\pm} = 0 \tag{75}$$

where g^+ is the damage surface function given in Eq. (40) and Δg^+ is the increment of the tensile damage function which is expressed by:

$$\Delta g^{\pm} = \frac{\partial g^{\pm}}{\partial Y_{ij}^{\pm}}\Delta Y_{ij}^{\pm} + \frac{\partial g^{\pm}}{\partial K^{\pm}}\Delta K^{\pm} \tag{76}$$

However, since $Y_{ij}^{\pm}$ is a function of $\sigma_{ij}^{\pm}$ and $\varphi_{ij}^{\pm}$ one can write the following:

$$\Delta Y_{ij}^{\pm} = \frac{\partial Y_{ij}^{\pm}}{\partial\sigma_{kl}^{\pm}}\Delta\sigma_{kl}^{\pm} + \frac{\partial Y_{ij}^{\pm}}{\partial\varphi_{kl}^{\pm}}\Delta\varphi_{kl}^{\pm} \tag{77}$$

where $\Delta\varphi_{kl}^{\pm}$ is obtained from Eqs. (A.20) and (A.21), such that:

$$\Delta\varphi_{kl}^{\pm} = \Delta\lambda_d^{\pm}\frac{\partial g^{\pm}}{\partial Y_{kl}^{\pm}} \tag{78}$$

and $\Delta\sigma_{kl}^{\pm}$ can be obtained from Eq. (22) as follows:

$$\Delta\sigma_{kl}^{\pm} = \frac{\partial M_{klrs}^{\pm}}{\partial\varphi_{mn}^{\pm}}\Delta\varphi_{mn}^{\pm}\bar{\sigma}_{rs}^{\pm} + M_{klrs}^{\pm}\Delta\bar{\sigma}_{rs}^{\pm} \tag{79}$$

By substituting Eqs. (77)–(79) into Eq. (76) and noticing that $\dot{\lambda}^{\pm} = \dot{\varphi}_{eq}^{\pm} = \sqrt{\dot{\varphi}_{ij}^{\pm}\dot{\varphi}_{ij}^{\pm}}$, one can obtain the following relation:

$$\Delta g^{\pm} = \frac{\partial g^{\pm}}{\partial Y_{ij}^{\pm}}\frac{\partial Y_{ij}^{\pm}}{\partial\sigma_{kl}^{\pm}}\frac{\partial M_{klrs}^{\pm}}{\partial\varphi_{mn}^{\pm}}\bar{\sigma}_{rs}^{\pm}\frac{\partial g^{\pm}}{\partial Y_{mn}^{\pm}}\Delta\lambda_d^{\pm} + \frac{\partial g^{\pm}}{\partial Y_{ij}^{\pm}}\frac{\partial Y_{ij}^{\pm}}{\partial\sigma_{kl}^{\pm}}M_{klrs}^{\pm}\Delta\bar{\sigma}_{rs}^{\pm} + \frac{\partial g^{\pm}}{\partial Y_{ij}^{\pm}}\frac{\partial Y_{ij}^{\pm}}{\partial\varphi_{kl}^{\pm}}\frac{\partial g^{\pm}}{\partial Y_{kl}^{\pm}}\Delta\lambda_d^{\pm} + \frac{\partial g^{\pm}}{\partial K^{\pm}}\frac{\partial K^{\pm}}{\partial\varphi_{eq}^{\pm}}\Delta\lambda_d^{\pm} \tag{80}$$

Substituting the above equation into Eq. (75), one obtains $\Delta\lambda_d^{\pm}$ by the following relation:

$$\Delta\lambda_d^{\pm} = \frac{g^{\pm tr}}{H_d^{\pm}} \tag{81}$$

where $g^{\pm tr}$ is the trial value of the damage function, $H_d^{\pm}$ is the tensile or compressive damage modulus and is given as follows:

$$H_d^{\pm} = \frac{\partial g^{\pm}}{\partial Y_{ij}^{\pm}} \frac{\partial Y_{ij}^{\pm}}{\partial \sigma_{kl}^{\pm}} \frac{\partial M_{klrs}^{\pm}}{\partial \varphi_{mn}^{\pm}} \bar{\sigma}_{rs}^{\pm} \frac{\partial g^{\pm}}{\partial Y_{mn}^{\pm}} + \frac{\partial g^{\pm}}{\partial Y_{ij}^{\pm}} \frac{\partial Y_{ij}^{\pm}}{\partial \varphi_{kl}^{\pm}} \frac{\partial g^{\pm}}{\partial Y_{kl}^{\pm}} + \frac{\partial g^{\pm}}{\partial K^{\pm}} \frac{\partial K^{\pm}}{\partial \varphi_{eq}^{\pm}} \tag{82}$$

where $\partial g/\partial K^{\pm} = -1$ and the expressions for $\partial g/\partial Y_{ij}$, $\partial Y_{ij}/\partial \sigma_{kl}$, $\partial M_{klrs}^{-1}/\partial \varphi_{mn}$, and $\partial Y_{ij}/\partial \varphi_{kl}$ can be found in Abu Al-Rub and Voyiadjis [2], whereas the expression of $\partial K/\partial \varphi_{eq}$ can be obtained from Eqs. (A.37) and (A.38) for the exponential and the power damage evolution laws, respectively.

4. Calibration and comparisons with experimental data

In order to investigate the predictive capability of the proposed model and the effectiveness of the numerical strategy, several numerical examples have been analyzed and comparisons with available experimental data have been made. The algorithmic model presented in the previous section is coded as a UMAT user material subroutine and implemented in the commercial finite element software ABAQUS. The response of the constitutive model is compared to results of experiments in loading–unloading, uniaxial, biaxial, and mixed mode fracture for different types of concrete. Details about the identification of the model material parameters are also presented.

4.1. Calibration of the compressive plasticity and damage evolution laws from loading–unloading uniaxial test

The identification of the plastic and damage material constants is commonly relied on monotonic stress–strain experimental curves in the field of continuum damage mechanics. Such an approach, however, results in a non-unique determination of these material constants. Therefore, a simple procedure for the identification of plasticity and damage material parameters is proposed here.

It is noteworthy that according to Eq. (32), compression plasticity material parameters seems to be needed in order to identify the tensile material parameters and vice versa. However, simplifying Eqs. (31) and (32) for the case of pure tension or pure compression, one can get an expression for the yield function independent of the compressive material parameters for pure tension (i.e. $f = \bar{\sigma}_{11}^{+} - c^{+} = 0$) and a yield function independent of the tensile material parameters for pure compression (i.e. $f = \bar{\sigma}_{11} - c^{-} = 0$). This allows one to indentify the tensile and compressive material parameters independently, which simplifies greatly the calibration procedure shown next.

Once the compressive yield strength f_0^- (at the start of the nonlinear behavior) is determined from monotonic or cyclic experimental results, the cyclic loading–unloading uniaxial compressive stress–strain experimental curve should then be used in identifying unique values for the material constants Q^- and b^- in Eq. $(35)_1$ and B^-, K_o^-, and q^- in Eqs. (48) and (52). Therefore, loading–unloading stress–strain data can be used to identify the material constants associated with the plasticity and damage constitutive equations simultaneously such that the reduction in Young's modulus can be used to identify the damage parameters. Once the damage law is calibrated, it can then be used to establish the effective stress–strain diagram which helps to identify the plasticity material constants in the effective (undamaged) configuration. This is demonstrated in the following subsections for some experimental loading–unloading compressive stress–strain diagrams. However, it is noteworthy that the values of Q^- and b^- are crucial for the evolution of the compressive damage density when using either the exponential or the power damage compressive evolution equations, Eqs. (48) and (52), and hence they are crucial for the accurate prediction of the nominal stress–strain relationship. For example, Figs. 3 and 4 show the evolution of the compressive damage density versus the applied strain by changing the values of the compressive plasticity hardening parameters Q^- and b^-, respectively. In the case of using the exponential damage evolution law, the damage evolution versus the applied strain, as expected, shows that the rate of damage growth is high initially and then decays to reach a constant value depending on Q^-. Meanwhile, when the power damage evolution law is used, the damage growth is slow initially and

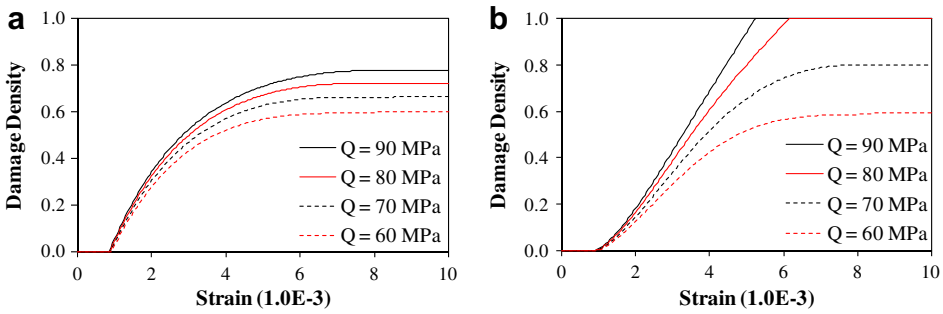

Fig. 3. Damage evolution according to the change of the compressive hardening modulus Q^- for: (a) exponential damage in Eq. (48), and (b) power damage in Eq. (52).

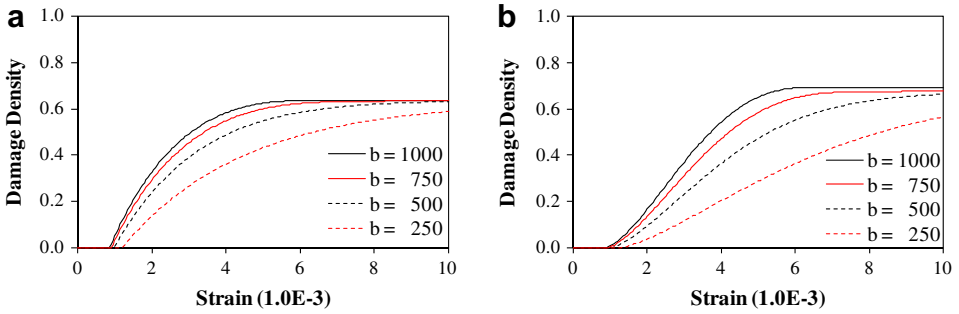

Fig. 4. Damage evolution according to the change of the compressive hardening rate constant b^- for: (a) exponential damage in Eq. (48), and (b) power damage in Eq. (52).

then increases with the strain, but decays at higher strains depending on the value of $Q^-$to give a desirable S-shape for the damage evolution. Moreover, for both damage evolution laws, the value of b^- affects the damage nucleation and growth rate whereas the value of Q^- affects the final damage value.

In order to show the procedure in indentifying the compressive plasticity and damage constitutive equation and compare the performance of the two compressive damage evolution laws presented in Eqs. (46) and (50), the compressive loading–unloading test results carried by Karsan and Jirsa [39] and Sinha et al. [71] are adopted.

4.1.1. Prediction of Karsan and Jirsa [39] experimental results

Since the plasticity constitutive equations are defined in the effective (undamaged) configuration, stress–strain data for an undamaged material is needed to indentify the plasticity material constants. One can establish such an effective stress–strain diagram from the nominal (damaged) loading–unloading stress–strain data by determining the damaged Young's modulus, E, for each cycle which is shown in Fig. 5. From Eqs. (8) and (9), one can define the effective stress $\bar{\sigma}$ as $\bar{\sigma} = (\bar{E}/E)\sigma$, where $\bar{E}$, E, and σ are measurable quantities such that at each unloading point (points A–E) the damaged Young's moduli are determined by connecting each unloading and reloading points (points A'–E'). As shown in Fig. 5, the experimental effective stress–strain shows an almost linear relation, and the predicted effective stress–strain curve is in close agreement with the experimental result. Based on this analysis, the compressive yield strength, f_0^-, compressive saturated hardening stress, Q^-, and the compressive hardening rate, b^-, although there can be numerous combinations, are determined as 15 MPa, 74 MPa, and 670 MPa, respectively. Moreover, from Eq. (9) and the measured damaged Young's modulus in Fig. 5, one can plot the variation of the damage density with strain as shown in Fig. 6b such that $\varphi = 1 - \sqrt{E/\bar{E}}$. Hence, these data can be used in identifying the damage parameters B^- and q^- and the damage threshold K_0^-.

The predicted nominal stress–strain curves and the damage densities using the exponential and power damage evolution laws as compared to the experimental results are shown in Figs. 6 and 7. The identified compressive plasticity and damage material constants are listed in Table 1. One can see that the power damage evolution law as in Fig. 7 gives much better predictions of both the nominal stress–strain diagram and the damage density as compared to the predictions of the exponential damage law as in Fig. 6. However, one may argue that the power damage law is associated with three material constants (B^-, q^-, and K_0^-) whereas the exponential damage law is as associated with only two material constants (B^- and K_0^-) such that one can obtain better predictions with more material constants. In fact, in this study, setting $q^- = 1$ (i.e. linear damage law) in

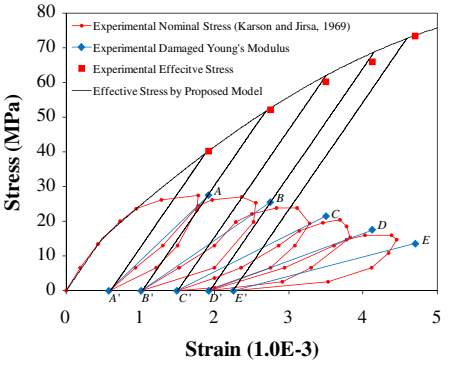

Fig. 5. Experimental analysis and predicted stress–strain diagrams in the effective (undamaged) and nominal (damaged) configurations for Karsan and Jirsa [39] experimental data.

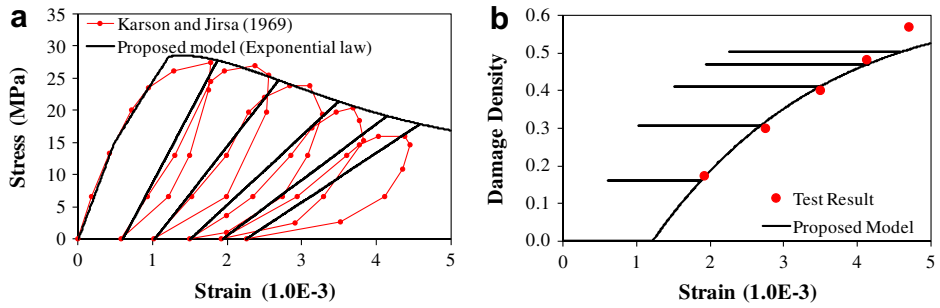

Fig. 6. Compressive loading–unloading analysis results of Karsan and Jirsa [39] experimental data when using the exponential damage law. (a) Nominal stress–strain curve, and (b) damage density.

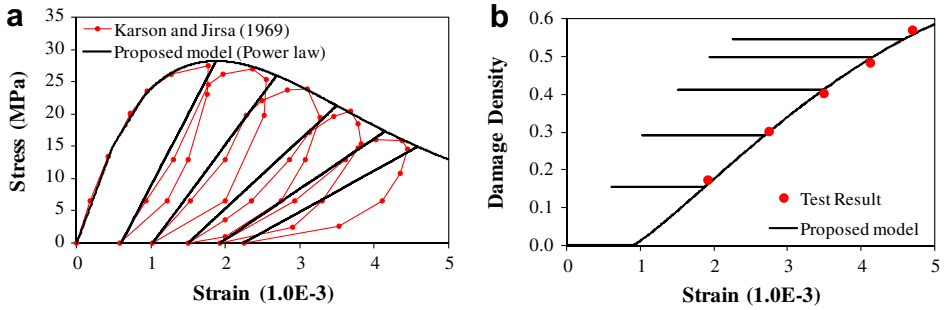

Fig. 7. Compressive loading–unloading analysis results of Karsan and Jirsa [39] experimental data when using the power damage law. (a) Nominal stress–strain curve, and (b) damage density.

Table 1
Material constants identified from the experimental results by Karson and Jirsa [39].

	$\bar{E}$ (MPa)	ν	f_0^- (MPa)	Q^- (MPa)	b^-	K_0^- (MPa)	B^-	q^-
Exponential law	31,000	0.2	15	74	670	25	0.45	–
Power law						20	0.22	1.16

all the numerical examples yielded much better predictions than the exponential damage law. Moreover, the smoothness of the stress–strain diagram, the accurate prediction of the damaged modulus, and the S-shape of the variation of the damage density with strain are highly desirable features that are predicted by the power damage law (or linear damage law when $q^- = 1$). However, one can notice that the experimental hysteretic loading–unloading behavior seen in Fig. 5 cannot be captured by the current model. In fact, to the author's best knowledge none of the existing concrete plasticity-damage models is capable of describing this hysteretic behavior.

4.1.2. Prediction of the experimental result by Sinha et al. [71]

Following the same procedure as in the previous subsection, the effective stress–strain diagram for the experimental result carried by Sinha et al. [71] is established from the nominal stress–strain loading–unloading diagram as shown in Fig. 8. The predicted effective stress–strain relation agrees well with the established effective stress–strain diagram if the values of the material constants f_0^-, Q^-, and b^- are identified as 14 MPa, 41 MPa, and 430 MPa, respectively. Furthermore, the compressive damage parameters are identified through fitting the established damage density versus strain from the nominal stress–strain loading–unloading experimental curve (see Fig. 9b). The identified compressive plasticity and damage material constants associated with fitting Karsan and Jirsa [39] experimental data are listed in Table 2. These constants are then used to predict the nominal stress–strain diagram and damage density as shown in Figs. 9 and 10 when using the exponential and power damage laws, respectively. It can be seen, as concluded from the previous analysis of Karsan and Jirsa [39] data, that the power damage evolution law gives a more accurate description of the softening part of the stress–strain diagram, degradation of the Young's modulus, and the S-shape curve for the damage density versus the applied strain.

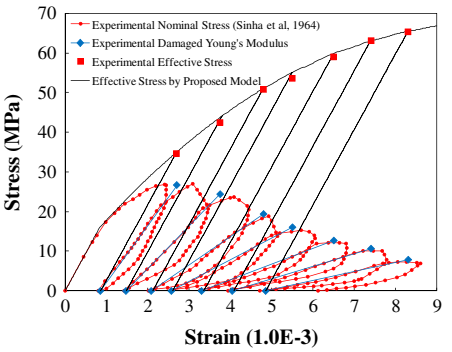

Fig. 8. Experimental analysis and predicted stress–strain diagrams in the effective (undamaged) and nominal (damaged) configurations for Sinha et al. [71] experimental data.

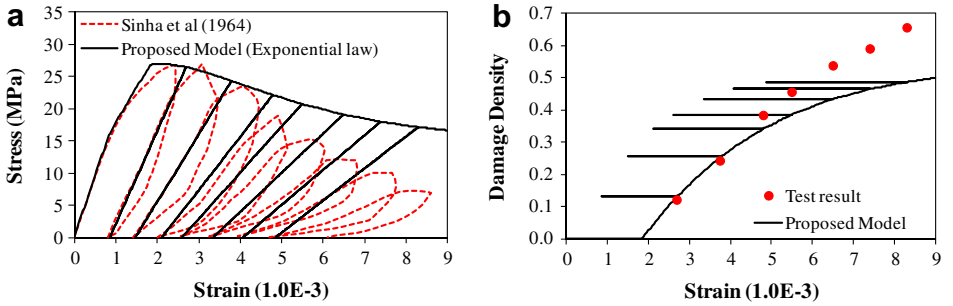

Fig. 9. Compressive loading–unloading analysis results of Sinha et al. [71] experimental data when using the exponential damage law. (a) Nominal stress–strain curve, and (b) damage density.

Table 2
Material constants identified from the experimental results of Sinha et al. [71].

	$\bar{E}$ (MPa)	ν	f_0^- (MPa)	Q^- (MPa)	b^-	K_0^- (MPa)	B^-	q^-
Exponential law	19,000	0.2	14	41	430	9	0.5	–
Power law						14.1	0.2	1.57

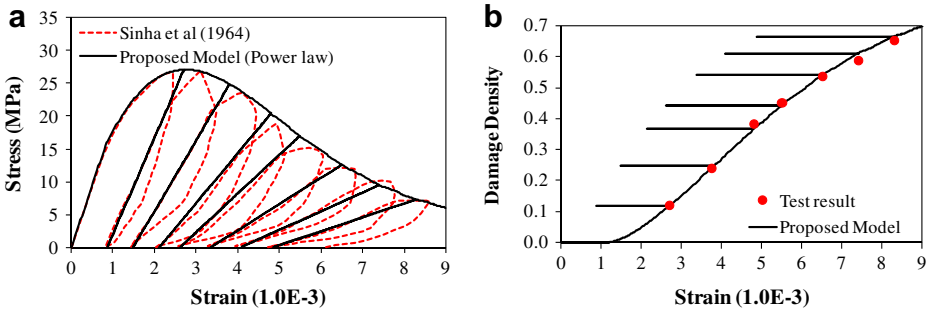

Fig. 10. Compressive loading–unloading analysis results of Sinha et al. [71] experimental data when using the power damage law. (a) Nominal stress–strain curve, and (b) damage density.

4.2. Calibration of the tensile plasticity and damage evolution laws from loading–unloading uniaxial tests

The procedure that is followed in Section 4.1 for the identification of the material constants associated with the compressive plasticity and damage constitutive equations is also followed here for calibration the tensile plasticity and damage constitutive equations. The loading–unloading uniaxial tensile tests by Taylor [72] are used in order to identify the material constants in Eqs. $(35)_2$, (47), and (51) (i.e. f_0^+, h^+, B^+, K_0^+, and q^+).

Figs. 11 and 12 show the analysis results where the identified material constants are listed in Table 3 for both exponential and power damage evolution laws, respectively. Although the two laws give similar results for the case of tensile loading, the power damage evolution law gives closer predictions of the softening part of the stress–strain diagram as compared to the corresponding prediction by the exponential damage evolution equation. For the result using the power damage law in Fig. 12a, the difference between the experimental and numerical stress–strain curve at the softening region still exists. This is because both the nominal stress–strain relation and the loading–unloading paths are considered simultaneously in calibrating the tensile constitutive equations. If the unloading parts are disregarded as in the case of monotonic uniaxial tensile loading, one can get a more precise prediction by using the power damage law, and those cases are considered in the next section.

As a result of the uniaxial loading–unloading tensile and compressive analysis, the power damage evolution law shows a better ability to predict the softening behavior of concrete for both compressive and tensile loading–unloading results. Therefore, the power damage evolution law, instead of the exponential damage law that has been used widely in the literature, is used in all of the following predictions and simulations.

4.3. Monotonic uniaxial compressive loading

Two different monotonic uniaxial compressive experimental results [39,83] are employed in this paper. The analysis results using the power damage evolution law are compared with the test results in Figs. 13 and 14, and the material constants used for the prediction of the two test results are listed in Table 4.

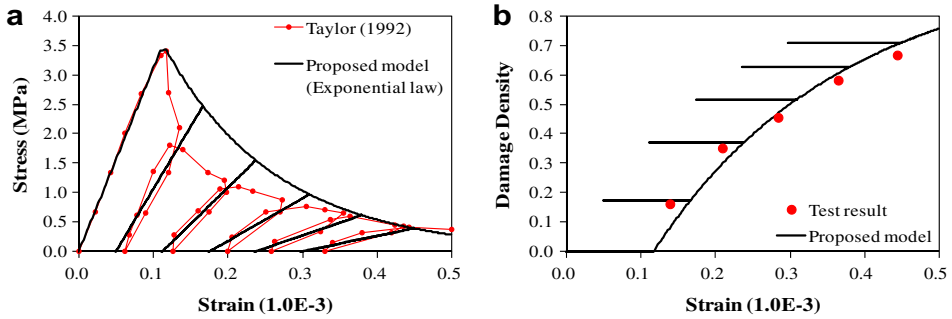

Fig. 11. Tensile loading–unloading analysis results of Taylor [72] experimental data when using the exponential damage law. (a) Nominal stress–strain curve, and (b) damage density.

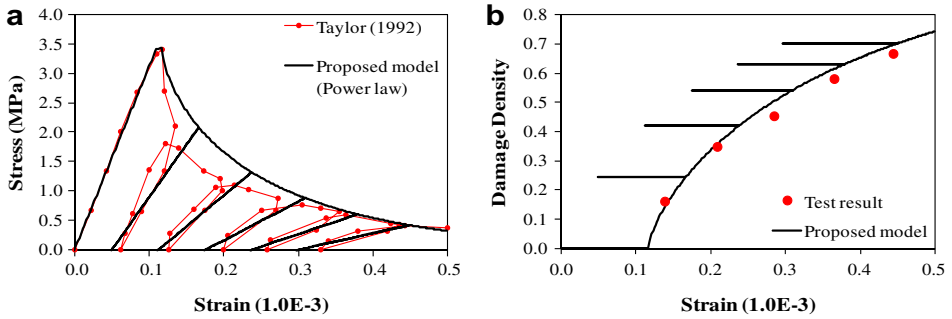

Fig. 12. Tensile loading–unloading analysis results of Taylor [72] experimental data when using the power damage law. (a) Nominal stress–strain curve, and (b) damage density.

Table 3
Material constants identified from the experimental data by Taylor [72].

	$\overline{E}$ (MPa)	ν	f_0^+ (MPa)	K_0^+ (MPa)	h^+ (MPa)	B^+	q^+
Exponential law	31,000	0.2	3.40	3.43	4,500	2.4	–
Power law						1.9	0.7

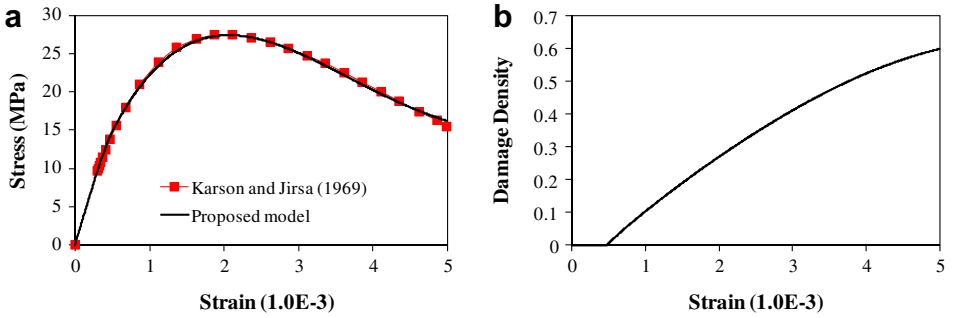

Fig. 13. Monotonic uniaxial compressive loading prediction of Karsan and Jirsa [39] experimental data. (a) Stress–strain relation, and (b) damage density.

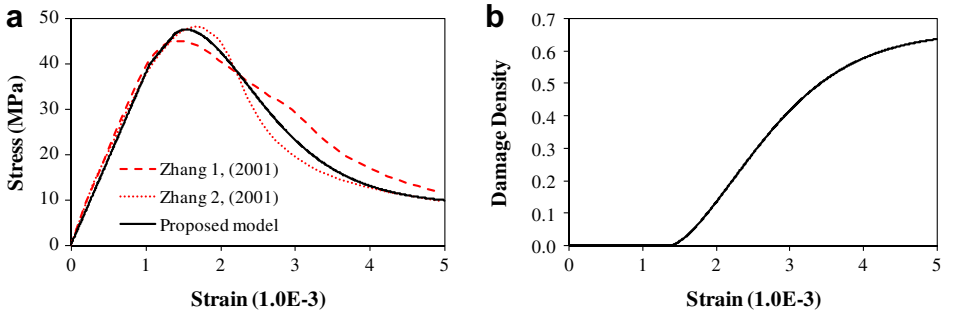

Fig. 14. Monotonic uniaxial compressive loading prediction of Zhang [83] experimental data. (a) Stress–strain relation, and (b) damage density.

Table 4
Material constants used for the monotonic uniaxial compressive loading analysis.

	$\overline{E}$ (MPa)	ν	f_0^- (MPa)	K_0^+ (MPa)	Q^- (MPa)	b^-	B^-	q^-
Karsan and Jirsa [39]	32,000	0.2	11	12.8	100	1350	0.11	0.93
Zhang [83]	38,000	0.2	40	41	36	1300	1.35	1.55

For both cases, the softening behaviors of concrete under compressive loading as well as the hardening regime are well predicted. However, it is noteworthy that since the loading–unloading experimental data are not available for uniaxial compressive loading for the concrete considered in Figs. 13 and 14a, which are crucial for identifying the material parameters of the compressive damage law, one may use another set of material constants in Table 4 to get analogous predictions. Hence, the loading–unloading experimental results are indispensable to obtain a unique set of material parameters. This is also true for the following monotonic uniaxial tensile loading predictions.

4.4. Monotonic uniaxial tensile loading

Two representative monotonic uniaxial tensile tests [24,83] are compared with the analysis results using the proposed tensile damage evolution law. The material constants used to predict the two test results are listed in Table 5, and Figs. 15 and 16 show the analysis results. As seen, the predicted nominal stress–strain relations by the proposed model using the power tensile damage evolution law are in close agreement with the experimental results.

Table 5
Material constants used for the monotonic uniaxial tensile loading analysis.

	$\overline{E}$ (MPa)	ν	f_0^+(MPa)	K_0^+(MPa)	h^+ (MPa)	B^+	q^+
Gopalaratnam and Shah [24]	31,000	0.2	3.45	3.52	15,000	1.4	0.6
Zhang [83]	34,000	0.2	3.39	3.4	4500	3.1	0.67

4.5. Monotonic biaxial compressive loading analysis

The biaxial compressive test results carried out by Kupfer et al. [43] are adopted in this paper in order to validate the proposed model. The analysis results are compared with the experimental results in Figs. 17a–c and the damage densities of

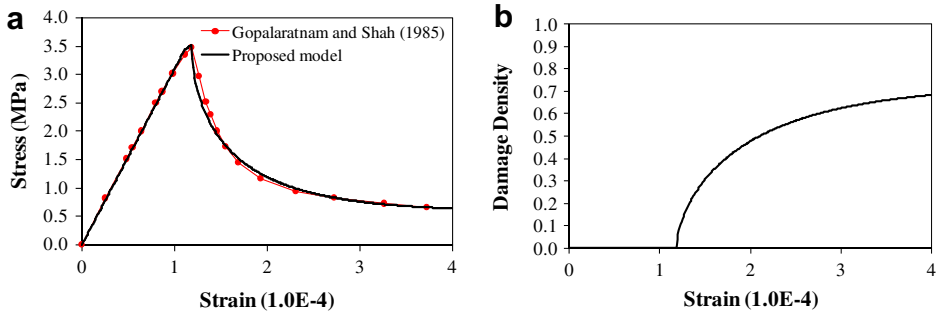

Fig. 15. Monotonic uniaxial tensile loading prediction of Gopalaratnam and Shah [24] experiment. (a) Stress–strain relation, and (b) damage density.

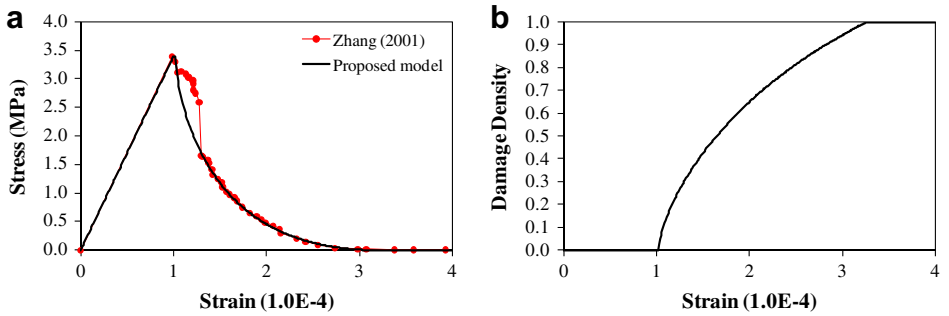

Fig. 16. Monotonic uniaxial tensile loading prediction of Zhang [83] experiment. (a) Stress–strain relation, and (b) damage density.

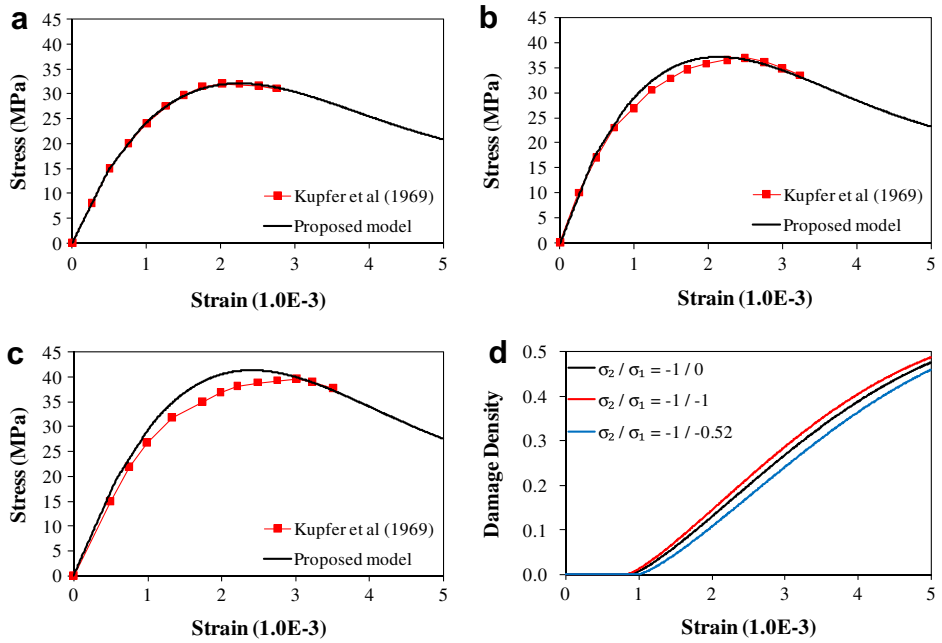

Fig. 17. The model response in uniaxial and biaxial compressive loading compared to experimental results reported by Kupfer et al. [43]. (a) $\sigma_2/\sigma_1 = -1/0$, (b) $\sigma_2/\sigma_1 = -1/-1$, (c) $\sigma_2/\sigma_1 = -1/-0.52$, and (d) damage density versus strain.

Table 6
Material constants used for the biaxial compressive loading analysis.

$\bar{E}$ (MPa)	v	f_0^- (MPa)	K_0^- (MPa)	Q^- (MPa)	b^-	B^-	q^-
29,000	0.2	15.0	20.0	70.0	810	0.16	1.29

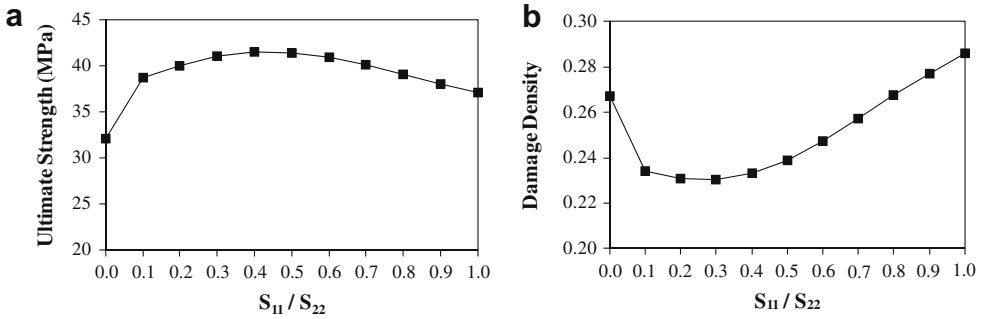

Fig. 18. Variation of the model response according to the change of the compressive biaxial stress ratio. (a) Ultimate compressive strength, and (b) damage density.

each case are compared in Fig. 17d. The material constants used in this simulation are listed in Table 6. Those material constants are determined from the monotonic uniaxial compressive loading test in Fig. 17a and then the same properties are used in predicting the biaxial compressive experimental results in Figs. 17b and c. The predicted results in Figs. 17b and c agree well with the test results although the ultimate stress is somewhat over predicted. Moreover, the damage density of the specimen under loading condition $\sigma_2/\sigma_1 = -1/-1$ is slightly higher than that of the specimen under uniaxial loading $\sigma_2/\sigma_1 = 1 - /0$, while the damage density of the specimen under the loading condition $\sigma_2/\sigma_1 = -1/-0.52$ is lower. This implies that the lump sum of damage densities in all directions is the highest for equi-biaxial compressive loading.

The variation of the ultimate compressive strength and the damage density according to the change of the biaxial stress ratio $S_{11}/S_{22} = \sigma_1/\sigma_2$ is shown in Fig. 18. For this analysis, the maximum transverse directional displacement δ_2 is fixed to -0.005 mm, and the maximum longitudinal displacement δ_1, considering the Poisson's effect, is varied from 0.001 mm to -0.005 mm for the biaxial stress ratio to be varied from 0 to 1. Each damage density in Fig. 18b is obtained at a strain level of 3×10^{-3}. One can notice that the ultimate compressive strength has a maximum value at a biaxial stress ratio of 0.4 while the damage density is minimum at a biaxial stress ratio of 0.3 and tends to increase as the biaxial stress ratio increases to a maximum value for equi-biaxial stress (i.e. stress ratio of 1) as concluded above. When the biaxial stress ratio is shifted from 0 to 0.1, both the ultimate compressive strength and the damage density of the element shows sudden change. This is due to the additional tensile damage induced by the longitudinal displacement δ_1 when the biaxial stress ratio is zero in order to maintain a zero biaxial stress ratio taking into consideration the Poisson's effect such that the tensile damage accelerates the transverse directional compressive damage.

4.6. Simulation of mixed-mode fracture of plain concrete

The mixed-mode fracture of the double-edge-notched (DEN) specimen tested by Nooru-Mohamed [56] is simulated to verify the efficiency of the proposed constitutive model. The geometry of the DEN specimens and the loading setup are presented in Fig. 19. The specimen dimensions are 200 mm $\times$ 200 mm square, 50 mm thick, and the length and height of the two notches are 25 mm and 5 mm, respectively. Although only two lading plates, top and left upper parts, were attached in the experimental set up, one more loading plate on the right upper part is attached additionally in the simulation in order to prevent the premature failure on the upper right and lower left-hand corners of the DEN specimen due to stress concentration. The vertical displacement δ_v of the specimen is an average displacement of $\delta_{MM'}$ and $\delta_{NN'}$.

Fig. 20 shows the plots of the initial mesh configurations. Three different mesh densities are used, and the size of the smallest element for coarse, middle, and fine meshes are 5.0 mm $\times$ 5.0 mm, 2.5 mm $\times$ 2.5 mm, and 1.25 mm $\times$ 1.25 mm, respectively. A three-dimensional (3D) eightnode linear brick element with one integration point is used. Although 3D simulations are performed, a 2 mm out-of-plane thickness is assumed instead of 50 mm actual thickness, and one element is taken through the thickness in order to reduce the simulation time. Same with the experimental set-up, bottom and right lower parts are fixed during whole loading steps, and a lateral (shear) force, P_S, is applied first up to the specified value of 5 kN or 10 kN with a zero vertical force, and then a vertical displacement, U, is loaded while P_S remains constant (see Fig. 19). The material parameters that are used in this simulation are listed in Table 7. These material constants are assumed

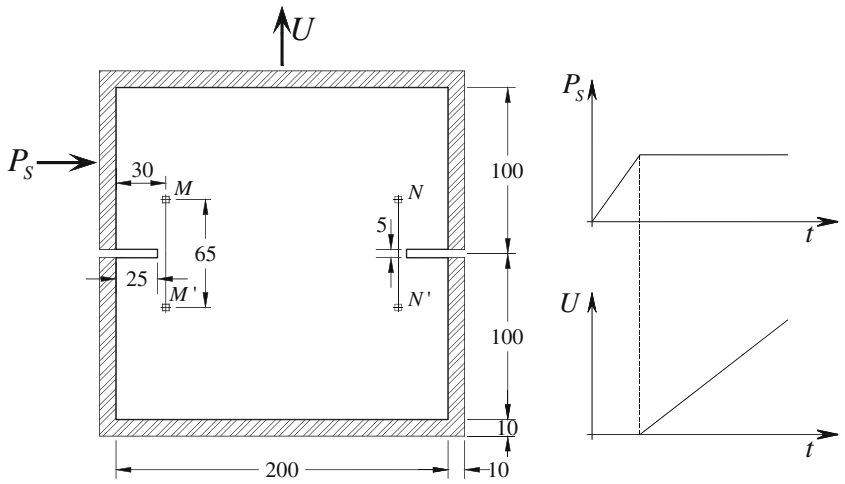

Fig. 19. Geometry and loading of the DEN specimen (units: mm).

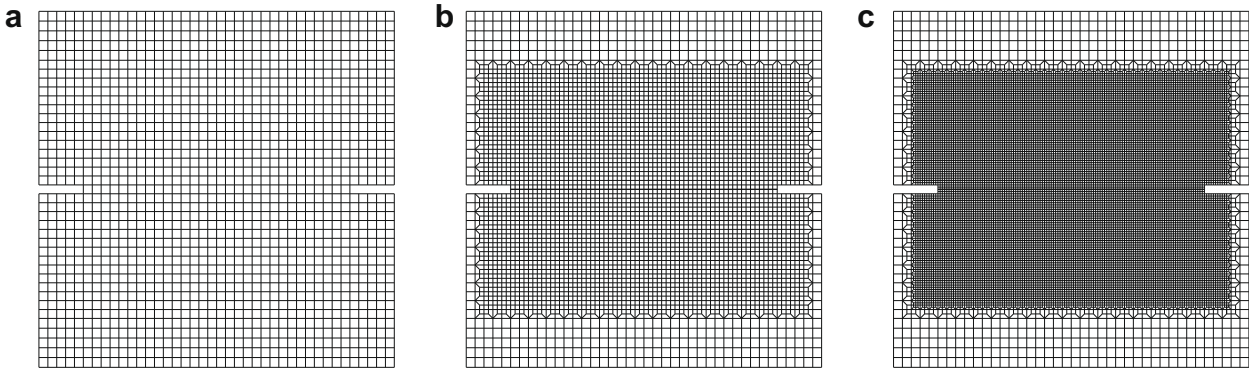

Fig. 20. Meshes used in the simulations: (a) coarse mesh (5.0 mm × 5.0 mm), (b) medium mesh (2.5 mm × 2.5 mm), and (c) fine mesh (1.25 mm × 1.25 mm).

Table 7
Material constants used for the DEN specimen fracture simulation.

Elastic constants		Yield criterion		Tensile material constants				
$\bar{E}$ (MPa)	v	α	α_p	f_0^+ (MPa)	K_0^+ (MPa)	h^+ (MPa)	B^+	q^+
30,000	0.2	0.12	0.2	3.5	3.55	4500	0.71	1.17

Compressive material constants					
f_0^- (MPa)	Q^- (MPa)	b^-	K_0^- (MPa)	B^-	q^-
15.0	120	1000	22	0.15	1.14

in light of the numerical comparisons in the previous sections and that matches qualitatively the observed experimental crack trajectories in Nooru-Mohamed [56].

The crack propagation for two loading cases are shown in Fig. 21 for the fine mesh, where the final shape of the crack patterns are compared to the crack patterns experimentally reported in Nooru-Mohamed [56] as overlapping each other. As shown, the initial slop of the crack increases in proportion to a rise in lateral shear force, P_S, and the trajectories of the crack of the analysis are in close agreement with the experimental results for both lateral loading cases. The tensile damage patterns for the three mesh densities are compared for both loading cases in Figs. 22 and 23. As can be shown, the model predicts qualitatively the crack patterns and trajectories almost independent of

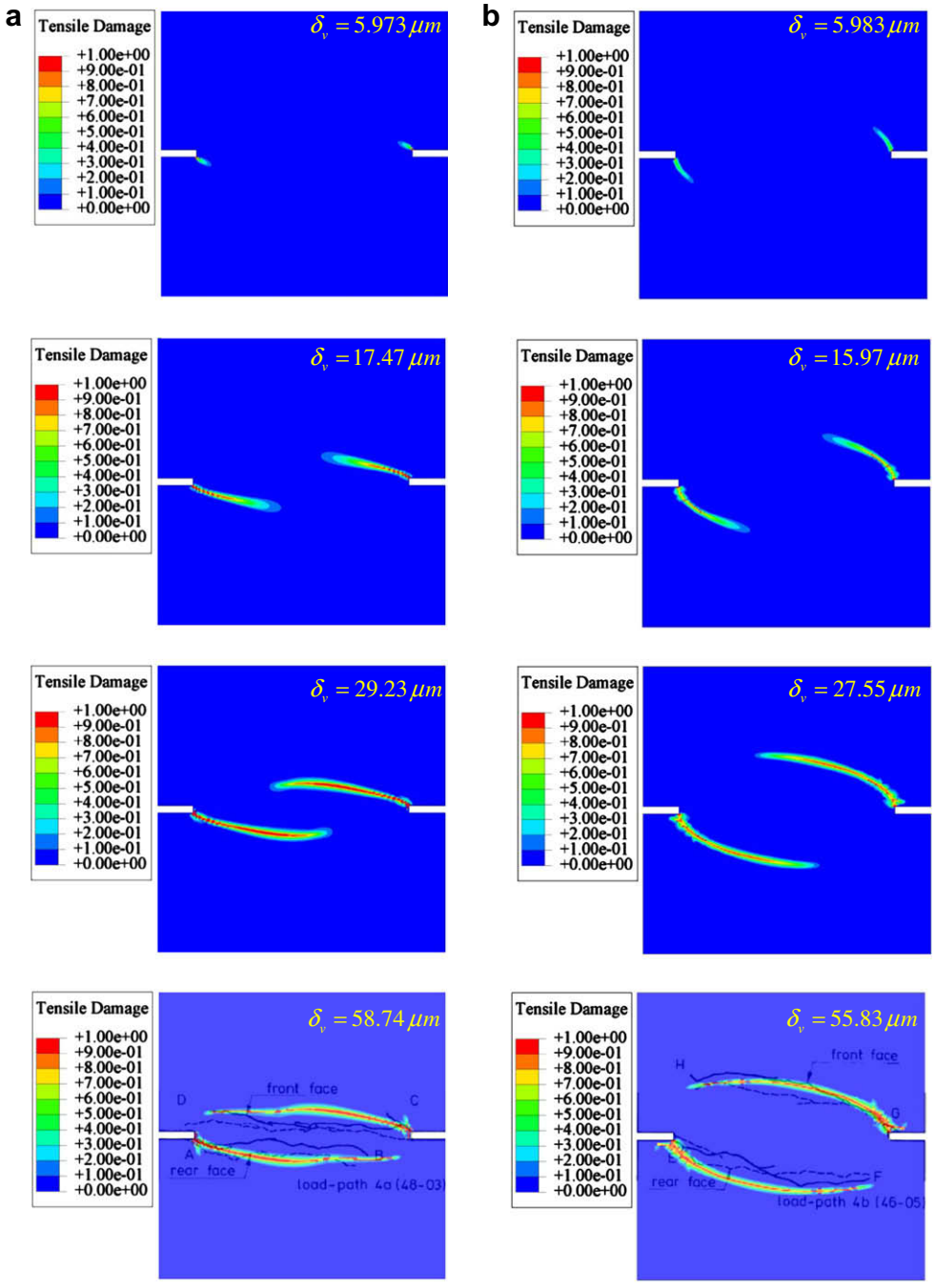

Fig. 21. Damage evolution showing the trend of crack propagation for two loading conditions: (a) P_S = 5.0 kN and (b) P_S = 10.0 kN. The figures at the bottom show the final crack propagation path as compared to the reported experiments by Nooru-Mohamed [56].

the mesh size. However, Fig. 24 shows plots of the reaction force versus the average displacement δ_v in which the solution is dependent on the mesh density; particularly, the ultimate load and the post-peak response. As the mesh density increases, the load capacity decreases due to damage localization and higher damage density. This implies that the proposed local constitutive model with damage localization and softening cannot provide an objective description of the failure results quantitatively, but to a less extent qualitatively. Therefore, the proposed constitutive model needs to be regularized by incorporating explicitly a material length scale parameter into the constitutive equations through the non-local damage approach as argued in Section 2.1. This is presented in detail for the current model in a separate publication [4].

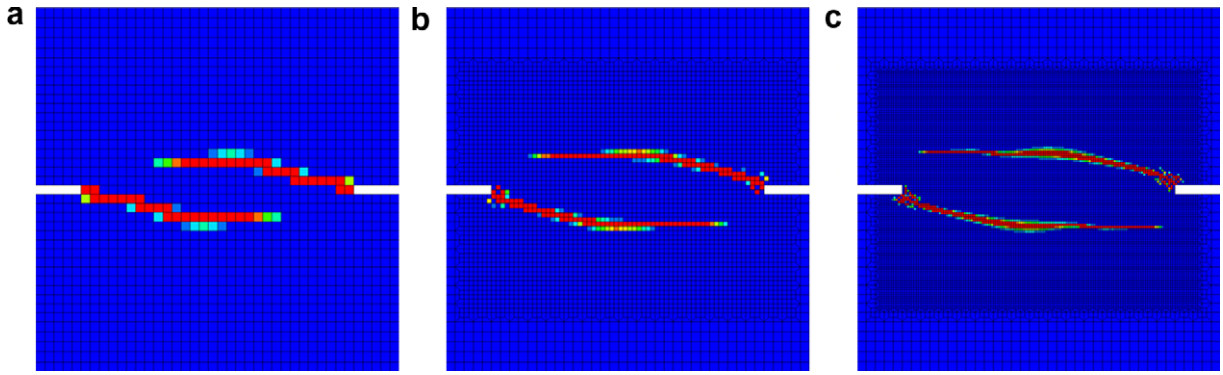

Fig. 22. Simulated crack trajectories for the load case $P_S = 5.0$ kN for three mesh densities: (a) coarse, (b) medium, and (c) fine.

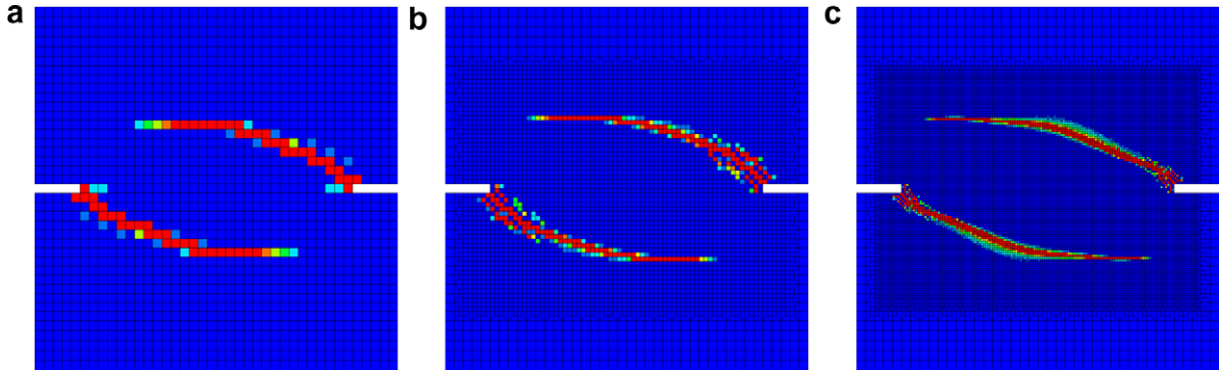

Fig. 23. Simulated crack trajectories for the load case $P_S = 10.0$ kN for three mesh densities: (a) coarse, (b) medium, and (c) fine.

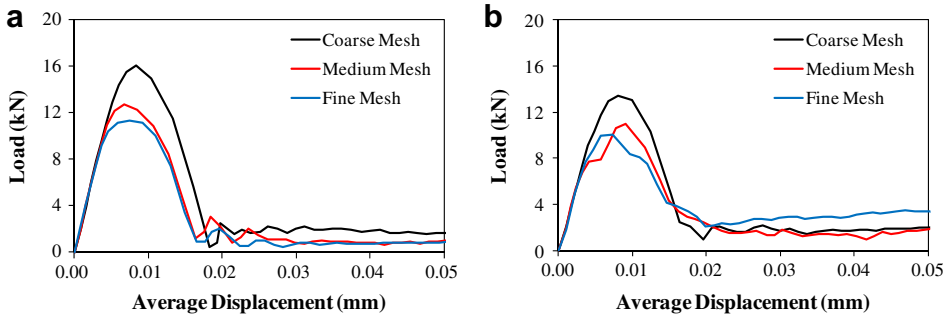

Fig. 24. Load versus displacement curves for different mesh densities and for the loading cases: (a) $P_S = 5.0$ kN, (b) $P_S = 10.0$ kN.

5. Conclusions

A coupled plasticity-damage model for plain concrete is presented in this paper. Based on continuum damage mechanics, the isotropic and anisotropic damage model is formulated on the basis of phenomenological observation that the damaged stiffness varies nonlinearly with the change of the damage density, where two different damage evolution laws for both tension and compression are proposed and examined for a more accurate prediction of the plain concrete behavior. The plasticity and damage loading surfaces account for both compressive and tensile loadings such that the tensile and compressive damages are characterized independently. The plasticity yield surface is expressed in the effective (undamaged) configuration, which leads to decoupled computational algorithms for the effective stress and the damage evolution. Also, it is shown that the proposed constitutive relations can be derived from the laws of thermodynamics. Numerical algorithms are presented for the implementation of the proposed model in the well-known finite element code ABAQUS through the material user subroutine UMAT.

It is concluded that the calibration of a plastic-damage model should be based on loading–unloading or cyclic test results since the plasticity material constants can then be identified from an easily established effective stress–strain diagram, whereas the damage material constants can be identified from the reduction in the Young's modulus. Hence, material constants that are identified from simple monotonic loading test cannot be used as reliable values for simulating the damage and failure of concrete structures that are subjected to various loading conditions. This is attributed to that these constants either underestimate or overestimate the plastic deformation and the level of damage density and degradation in the structural stiffness such that there is no way to tell from these simple uniaxial monotonic tests that if plasticity or damage are overestimated or underestimated.

The overall performance of the proposed model is tested by comparing the model predictions to experimental data. It is shown that the proposed model using the power damage evolution law gives a better prediction than the model using the exponential damage evolution law through the uniaxial loading–unloading tension and compression analyses. Additional experimental simulations of concrete response, using the power damage evolution law, under various loading conditions, such as monotonic uniaxial tension and compression and monotonic biaxial compression, also show close agreement with the experimental results. Furthermore, the numerical simulation of the mixed-mode fracture of DEN specimen agrees well with the test data. This shows that the proposed model with corporation of plasticity and damage provides an effective method for modeling the concrete behavior under various loading conditions such that the model is suitable for three-dimensional structural concrete applications.

However, the presented local constitutive relations result in an ill-posed boundary value problem for material softening. Consequently, the uniqueness of the solution for the problem is not guaranteed such that the mesh dependent results in the finite element analysis are seen. Therefore, a localization limiter such as the strain gradient theory [78] should be adopted as a remedy to this problem. Furthermore, the strain energy equivalence hypothesis, as opposed to the hypothesis of the strain equivalence which is adapted in this work, will be used in a future study to develop strongly and explicitly coupled plastic-damage constitutive equations and compare them to the current implicitly coupled plastic-damage constitutive equations.

Acknowledgment

Financial support by the Texas Southwest University Transportation Center (SWUTC) is gratefully acknowledged.

Appendix A

Here, the proposed elasto-plastic-damage model is derived using a thermodynamic consistent framework. The Helmholtz free energy can be expressed in terms of a suitable set of internal state variables that characterize the elastic, plastic, and damage behavior of concrete. In this paper the following internal variables are assumed to satisfactory characterize the concrete behavior both in tension and compression, such that:

$$\psi = \psi\left(\varepsilon^e_{ij},\ \varphi^+_{ij},\ \varphi^-_{ij},\ \varphi^+_{eq},\ \varphi^-_{eq},\ \varepsilon^+_{eq},\ \varepsilon^-_{eq}\right) \tag{A.1}$$

where φ^+_{eq} and φ^-_{eq} are the equivalent (accumulated) damage variables for tension and compression , respectively, which are defined as $\varphi^\pm_{eq} = \int_0^t \dot{\varphi}^\pm_{eq}\mathrm{d}t$. Similarly, ε^+_{eq} and ε^-_{eq} are the equivalent tensile and compressive plastic strains that are used here to characterize the plasticity isotropic hardening, $\varepsilon^\pm_{eq} = \int_0^t \dot{\varepsilon}^\pm_{eq}\mathrm{d}t$.

The Helmholtz free energy is given as a decomposition of elastic ψ^e, plastic ψ^p, and damage ψ^d, parts, such that:

$$\psi = \psi^e(\varepsilon^e_{ij},\ \varphi^+_{ij},\ \varphi^-_{ij}) + \psi^p(\varepsilon^+_{eq},\ \varepsilon^-_{eq}) + \psi^d(\varphi^+_{eq},\ \varphi^-_{eq}) \tag{A.2}$$

It can be noted from the above decomposition that damage affects only the elastic properties and not the plastic ones. However, for a more realistic description, one should introduce the damage variables in the plastic part of the Helmholtz free energy (see [2]). However, these effects are not significant for brittle materials and can, therefore, be neglected.

The elastic free energy ψ^e is given in term of the second-order damage tensors $\varphi^\pm_{ij}$ as follows:

$$\psi^e = \frac{1}{2}\varepsilon^e_{ij}E_{ijkl}(\varphi^+_{ij},\varphi^-_{ij})\varepsilon^e_{kl} = \frac{1}{2}\sigma_{ij}\varepsilon^e_{ij} = \frac{1}{2}(\sigma^+_{ij}+\sigma^-_{ij})\varepsilon^e_{ij} = \frac{1}{2}M_{ijpq}\bar{\sigma}_{pq}\varepsilon^e_{ij} \tag{A.3}$$

where M_{ijpq} is given in Eq. (26).

The Clausius–Duhem inequality for isothermal case is given as follows:

$$\sigma_{ij}\dot{\varepsilon}_{ij} - \rho\dot{\psi} \geqslant 0 \tag{A.4}$$

where ρ is the material density. Taking the time derivative of Eq. (A.2), the following expression can be written:

$$\dot{\psi} = \frac{\partial\psi^e}{\partial\varepsilon^e_{ij}}\dot{\varepsilon}^e_{ij} + \frac{\partial\psi^e}{\partial\varphi^+_{ij}}\dot{\varphi}^+_{ij} + \frac{\partial\psi^e}{\partial\varphi^-_{ij}}\dot{\varphi}^-_{ij} + \frac{\partial\psi^p}{\partial\varepsilon^+_{eq}}\dot{\varepsilon}^+_{eq} + \frac{\partial\psi^p}{\partial\varepsilon^-_{eq}}\dot{\varepsilon}^-_{eq} + \frac{\partial\psi^d}{\partial\varphi^+_{eq}}\dot{\varphi}^+_{eq} + \frac{\partial\psi^d}{\partial\varphi^-_{eq}}\dot{\varphi}^-_{eq} \tag{A.5}$$

By plugging the above equation into the Clausius–Duhem inequality, A.4), and making some simplifications, one can obtain the following relations for any admissible state variables, such that:

$$\sigma_{ij} = \rho \frac{\partial \psi^e}{\partial \varepsilon^e_{ij}} \tag{A.6}$$

and

$$\sigma_{ij}\dot{\varepsilon}^p_{ij} + Y^+_{ij}\dot{\varphi}^+_{ij} + Y^-_{ij}\dot{\varphi}^-_{ij} - c^+\dot{\varepsilon}^+_{eq} - c^-\dot{\varepsilon}^-_{eq} - K^+\dot{\varphi}^+_{eq} - K^-\dot{\varphi}^-_{eq} \geqslant 0 \tag{A.7}$$

where the damage and plasticity conjugate forces that appear in the above expression are defined as follows:

$$Y^+_{ij} = -\rho \frac{\partial \psi^e}{\partial \varphi^+_{ij}} \tag{A.8}$$

$$Y^-_{ij} = -\rho \frac{\partial \psi^e}{\partial \varphi^-_{ij}} \tag{A.9}$$

$$K^+ = \rho \frac{\partial \psi^d}{\partial \varphi^+_{eq}} \tag{A.10}$$

$$K^- = \rho \frac{\partial \psi^d}{\partial \varphi^-_{eq}} \tag{A.11}$$

$$c^+ = \rho \frac{\partial \psi^p}{\partial \varepsilon^+_{eq}} \tag{A.12}$$

$$c^- = \rho \frac{\partial \psi^p}{\partial \varepsilon^-_{eq}} \tag{A.13}$$

Therefore, one can rewrite the Clausius-Duhem inequality in Eq. (A.7) to yield the dissipation energy, Π, due to plasticity, Π^p, and damage, Π^d, as follows:

$$\Pi = \Pi^d + \Pi^p \geqslant 0 \tag{A.14}$$

with

$$\Pi^p = \sigma_{ij}\dot{\varepsilon}^p_{ij} - c^+\dot{\varepsilon}^+_{eq} - c^-\dot{\varepsilon}^-_{eq} \geqslant 0 \tag{A.15}$$

$$\Pi^d = Y^+_{ij}\dot{\varphi}^+_{ij} + Y^-_{ij}\dot{\varphi}^-_{ij} - K^+\dot{\varphi}^+_{eq} - K^-\dot{\varphi}^-_{eq} \geqslant 0 \tag{A.16}$$

The rate of the internal variables associated with plastic and damage deformations are obtained by utilizing the calculus of functions of several variables with the plasticity and damage Lagrangian multipliers, $\dot{\lambda}^p$ and $\dot{\lambda}^\pm_d$, such that the following objective function can be defined (see Abu Al-Rub and Voyiadjis [2] for more details about this step):

$$\Omega = \Pi - \dot{\lambda}^p F^p - \dot{\lambda}^+_d g^+ - \dot{\lambda}^-_d g^- \geqslant 0 \tag{A.17}$$

Using the well known maximum dissipation principle [67,68], which states that the actual state of the thermodynamic forces (σ_{ij}, $Y^\pm_{ij}$, $c^\pm$, $K^\pm$) are that which maximizes the dissipation function over all other possible admissible states, one can maximize the objective function Ω by using the necessary conditions as follows:

$$\frac{\partial \Omega}{\partial \sigma_{ij}} = 0, \quad \frac{\partial \Omega}{\partial Y^\pm_{ij}} = 0, \quad \frac{\partial \Omega}{\partial c^\pm} = 0, \quad \frac{\partial \Omega}{\partial K^\pm} = 0 \tag{A.18}$$

Substituting Eq. (A.17) along with Eqs. (A.15) and (A.16) into (A.18) yield the following thermodynamic plasticity and damage flow rules:

$$\dot{\varepsilon}^p_{ij} = \dot{\lambda}^p \frac{\partial F^p}{\partial \sigma_{ij}} \tag{A.19}$$

$$\dot{\varphi}^+_{ij} = \dot{\lambda}^+_d \frac{\partial g^+}{\partial Y^+_{ij}} \tag{A.20}$$

$$\dot{\varphi}^-_{ij} = \dot{\lambda}^-_d \frac{\partial g^-}{\partial Y^-_{ij}} \tag{A.21}$$

$$\dot{\varepsilon}^+_{eq} = \dot{\lambda}^p \frac{\partial F^p}{\partial c^+} \tag{A.22}$$

$$\dot{\varepsilon}^-_{eq} = \dot{\lambda}^p \frac{\partial F^p}{\partial c^-} \tag{A.23}$$

$$\dot{\varphi}^+_{eq} = \dot{\lambda}^+_d \frac{\partial g^+}{\partial K^+} \tag{A.24}$$

$$\dot{\varphi}^-_{eq} = \dot{\lambda}^-_d \frac{\partial g^-}{\partial K^-} \tag{A.25}$$

The elastic part of the Helmholtz free energy function, ψ^e, as presented in Eq. (A.3) can be substituted into Eq. (A.6) to yield the following stress–strain relation:

$$\sigma_{ij} = E_{ijkl}\varepsilon^e_{kl} = E_{ijkl}(\varepsilon_{kl} - \varepsilon^p_{kl}) \tag{A.26}$$

Now, one can obtain expressions for the damage driving forces $Y^{\pm}_{ij}$ from Eqs. (A.3), (A.8) and (A.9) as follows:

$$Y^{\pm}_{rs} = -\frac{1}{2}\varepsilon^e_{ij}\frac{\partial E_{ijkl}}{\partial \varphi^{\pm}_{rs}}\varepsilon^e_{kl} \tag{A.27}$$

By taking the derivative of Eq. (21) with respect to the damage parameter $\varphi^{\pm}_{ij}$ one obtains:

$$\frac{\partial E_{ijkl}}{\partial \varphi^{\pm}_{rs}} = \frac{\partial M_{ijmn}}{\partial \varphi^{\pm}_{rs}}\bar{E}_{mnkl} \tag{A.28}$$

Now, by substituting Eq. (A.28) into Eq. (A.27), one obtains the following expression for $Y^{\pm}_{ij}$:

$$Y^{\pm}_{rs} = -\frac{1}{2}\varepsilon^e_{ij}\frac{\partial M_{ijmn}}{\partial \varphi^{\pm}_{rs}}\bar{E}_{mnkl}\varepsilon^e_{kl} \tag{A.29}$$

where from Eq. (26), one can write the following expression:

$$\frac{\partial M_{ijmn}}{\partial \varphi^{\pm}_{rs}} = \frac{\partial M^{\pm}_{ijpq}}{\partial \varphi^{\pm}_{rs}}P^{\pm}_{pqmn} \tag{A.30}$$

One can also rewrite Eq. (A.29) in terms of the effective stress tensor $\bar{\sigma}_{ij}$ by replacing ε^e_{kl} from Eq. $(18)_2$ as follows:

$$Y^{\pm}_{rs} = -\frac{1}{2}\bar{E}^{-1}_{ijab}\bar{\sigma}_{ab}\frac{\partial M_{ijpq}}{\partial \varphi^{\pm}_{rs}}\bar{\sigma}_{pq} \tag{A.31}$$

The plastic part of the Helmholtz free energy function is postulated to have the following form Abu Al-Rub and Voyiadjis [2]:

$$\rho\psi^p = f^+_0\varepsilon^+_{eq} + \frac{1}{2}h^+(\varepsilon^+_{eq})^2 + f^-_0\varepsilon^-_{eq} + Q^-\left[\varepsilon^-_{eq} + \frac{1}{b^-}\exp(-b^-\varepsilon^-_{eq})\right] \tag{A.32}$$

Substituting Eq. (A.32) into Eqs. (A.18) and (A.19) yields the following expressions for the plasticity conjugate forces c^+ and c^- that are equal to Eq. (35):

$$c^+ = f^+_0 + h^+\varepsilon^+_{eq} \tag{A.33}$$

$$c^- = f^-_0 + Q^-\left[1 - \exp(-b^-\varepsilon^-_{eq})\right] \tag{A.34}$$

The damage part of the Helmholtz free energy functions for the exponential and the power damage evolution laws that are presented in Section 2.6 are postulated to have the following form:

(1) for the exponential damage evolution law

$$\rho\psi^d = K^{\pm}_0\left[\varphi^{\pm}_{eq} + \frac{1}{B^{\pm}}\left\{(1-\varphi^{\pm}_{eq})\ln(1-\varphi^{\pm}_{eq}) + \varphi^{\pm}_{eq}\right\}\right] \tag{A.35}$$

(2) for the power damage evolution law

$$\rho\psi^d = K^{\pm}_0\left[\varphi^{\pm}_{eq} + \left(\frac{q^{\pm}}{q^{\pm}+1}\right)\left(\frac{1}{B^{\pm}}\right)^{q^{\pm}}\varphi^{\frac{1}{q^{\pm}}+1}_{eq}\right] \tag{A.36}$$

where $K^{\pm}_0$ is the initial damage threshold and $B^{\pm}$ are material constants which are expressed in terms of the fracture energy.

Substituting Eq. (A.35) into Eqs. (A.10) and (A.11), the following expressions for the damage forces $K^{\pm}$ for the exponential damage evolution law can be easily obtained as:

$$K^{\pm} = K^{\pm}_0\left[1 - \frac{1}{B^{\pm}}\ln(1-\varphi^{\pm}_{eq})\right] \tag{A.37}$$

Similarly, one can derive the damage forces $K^{\pm}$ for the power damage evolution law by substituting Eq. (A.36) into Eqs. (A.10) and (A.11) as follows:

$$K^{\pm} = K^{\pm}_0\left[1 + \left(\frac{1}{B^{\pm}}\varphi^{\pm}_{eq}\right)^{\frac{1}{q^{\pm}}}\right] \tag{A.38}$$

By taking the time derivative of Eqs. (A.37) and (A.38) separately, one retrieves the rate form of the damage function $\dot{K}^{\pm}$ for the exponential and the power damage evolution laws presented in Eqs. (47)–(52), such that:

(1) for the exponential damage evolution law

$$\dot{K}^{\pm} = \frac{K_0^{\pm}}{B^{\pm}} \exp\left[-B^{\pm}\left(1 - \frac{K^{\pm}}{K_0^{\pm}}\right)\right] \dot{\varphi}_{eq}^{\pm} \tag{A.39}$$

(2) for the power damage evolution law

$$\dot{K}^{\pm} = \frac{K_0^{\pm}}{B^{\pm} q^{\pm}} \left[\frac{K^{\pm}}{K_0^{\pm}} - 1\right]^{1-q^{\pm}} \dot{\varphi}_{eq}^{\pm} \tag{A.40}$$

It is noteworthy that the expressions of the tensile damage functions K^{+} for the exponential and the power damage evolution laws presented in Eqs. (47) and (51), are slightly different than the expressions shown in Eqs. (A.39) and (A.40). However, in this study, Eqs. (47) and (51) are used. This is attributed to their better representation of the stress–strain diagram under tensile loading.

References

[1] ABAQUS Ver 6.5. Providence, RI: Habbitt, Karlsson and Sorensen, Inc.
[2] Abu Al-Rub RK, Voyiadjis GZ. On the coupling of anisotropic damage and plasticity models for ductile materials. Int J Solids Struct 2003;40:2611–43.
[3] Abu Al-Rub RK, Voyiadjis GZ. A finite strain plastic-damage model for high velocity impacts using combined viscosity and gradient localization limiters, Part I: theoretical formulation. Int J Damage Mech 2006;15:293–334.
[4] Abu Al-Rub RK, Voyiadjis GZ. Gradient-enhanced coupled plasticity-anisotropic damage model for concrete fracture: computational aspects and applications. Int J Damage Mech 2009;18:115–54.
[5] Ananiev S, Ožbolt J. Plastic-damage model for concrete in principal directions. In: Li V, Leung CKY, William KJ, Billington SL, editors. Fracture mechanics of concrete structures; 2004. p. 271–8.
[6] Bazant ZP, Kim S-S. Plastic-fracturing theory for concrete. J Engng Mech Div (ASCE) 1979;105:407–28.
[7] Bazant ZP. On endochronic inelasticity and incremental plasticity. Int J Solids Struct 1978;14:691–714.
[8] Carol I, Rizzi E, William KJ. On the formulation of anisotropic elastic degradation. II. Generalized pseudo-Rankine model for tensile damage. Int J Solids Struct 2001;38:519–46.
[9] Cervenka J, Papanikolaou VK. Three dimensional combined fracture – plastic material model for concrete. Int J Plasticity 2008;24:2192–220.
[10] Chen ACT, Chen WF. Constitutive relations for concrete. J Engng Mech Div (ASCE) 1975;101:465–81.
[11] Chen ES, Buyukozturk O. Constitutive model for concrete in cyclic compression. J Engng Mech Div (ASCE) 1985;111:797–814.
[12] Chow CL, Wang J. An anisotropic theory of elasticity for continuum damage mechanics. Int J Fract 1987;33:2–16.
[13] Cicekli U, Voyiadjis GZ, Abu Al-Rub RK. A plastic and anisotropic damage model for plain concrete. Int J Plasticity 2007;23:1874–900.
[14] Coleman BD, Gurtin ME. Thermodynamics with internal state variables. J Chem Phys 1967;47(2):597–613.
[15] Comi C. A non-local model with tension and compression damage mechanisms. Eur J Mech A/Solids 2001;20:1–22.
[16] Contrafatto L, Cuomo M. A framework of elastic–plastic damaging model for concrete under multiaxial stress states. Int J Plasticity 2006;22:2272–300.
[17] Cordebois JP, Sidoroff F. Anisotropic damage in elasticity and plasticity. J Mec Theor Appl 1979:40–5 [Numero Special].
[18] Di Luzio G. Asymmetric over-nonlocal microplane model M4 for fracture in concrete. Int J Solids Struct 2007;44:4418–41.
[19] Dragon A, Mroz Z. A continuum model for plastic-brittle behavior of rock and concrete. Int J Engng Sci 1979;17:121–37.
[20] de Borst R, Pamin J, Peerlings RHJ, Sluys LJ. On gradient-enhanced damage and plasticity models for failure in quasibrittle and frictional materials. Comput Mech 1995;17:130–41.
[21] Este G, Willam KJ. A fracture-energy based constitutive formulation for inelastic behavior of plain concrete. J Engng Mech ASCE 1994;120:1983–2011.
[22] Feenstra PH, de Borst R. A composite plasticity model for concrete. Int J Solids Struct 1996;33:707–30.
[23] Gatuingt F, Pijaudier-Cabot G. Coupled damage and plasticity modeling in transient dynamic analysis of concrete. Int J Numer Anal Methods Geomech 2002;26:1–24.
[24] Gopalaratnam VS, Shah SP. Softening response of plain concrete in direct tension. ACI J 1985;85:310–23.
[25] Grassl P, Jirasek M. Plastic model with non-local damage applied to concrete. Int J Numer Anal Methods Geomech 2006;30:71–90.
[26] Grassl P, Lundgren K, Gylltoft K. Concrete in compression: a plasticity theory with a novel hardening law. Int J Solids Struct 2002;39:5205–23.
[27] Hansen E, William K, Carol I. A two-surface anisotropic damage/plasticity model for plain concrete. In: de Borst R, Mazars J, Pijaudier-Cabot G, van Mier JGM, editors. Fracture mechanics of concrete structures. Lisse: Balkema; 2001. p. 549–56.
[28] Imran I, Pantazopoulu SJ. Plasticity model for concrete under triaxial compression. J Engng Mech 2001;127:281–90.
[29] Jason L, Pijaudier-Cabot G, Huerta A, Crouch R, Ghavamian S. An elastic plastic damage formulation for the behavior of concrete. In: Li V, Leung CKY, William KJ, Billington SL, editors. Fracture mechanics of concrete structures; 2004. p. 549–56.
[30] Jefferson AD. Craft – a plastic-damage-contact model for concrete. I. Model theory and thermodynamic considerations. Int J Solids Struct 2003;40:5973–99.
[31] Jefferson AD. Craft – a plastic-damage-contact model for concrete. II. Model implementation with implicit return-mapping algorithm and consistent tangent matrix. Int J Solids Struct 2003;40:6001–22.
[32] Jirasek M. Nonlocal models for damage and fracture: comparison of approaches. Int J Solids Struct 1998;35:4133–45.
[33] Ju JW. On energy-based coupled elasto-plastic damage theories: constitutive modeling and computational aspects. Int J Solids Struct 1989;25:803–33.
[34] Ju JW. Isotropic and anisotropic damage variables in continuum damage mechanics. J Engng Mech ASCE 1990;116:2764–70.
[35] Kachonov LM. On the creep fracture time. Izv Akad Nauk USSR Otd Tech 1958;8:26–31 [in Russian].
[36] Kattan PI, Voyiadjis GZ. Decomposition of damage tensor in continuum damage mechanics. J Engng Mech 2001;127:940–4.
[37] Kratzig W, Polling R. An elasto-plastic damage model for reinforced concrete with minimum number of material parameters. Comput Struct 2004;82:1201–15.
[38] Karabinis AI, Kiousis PD. Effects of confinement on concrete columns: a plasticity theory approach. ASCE J Struct Engng 1994;120:2747–67.
[39] Karsan ID, Jirsa JO. Behavior of concrete under compressive loadings. J Engng Mech Div (ASCE) 1969;95:2535–63.
[40] Krajcinovic D. Continuum damage mechanics. Appl Mech Rev 1983;37:1–6.
[41] Krajcinovic D. Continuous damage mechanics revisited: basic concepts and definitions. J Appl Mech 1985;52:829–34.
[42] Krajcinovic D. Damage mechanics. Amsterdam: North-Holland; 1996.

[43] Kupfer H, Hilsdorf HK, Rusch H. Behavior of concrete under biaxial stresses. ACI J 1969;66:656–66.
[44] Lee J, Fenves GL. A plastic-damage model for cyclic loading of concrete structures. J Engng Mech ASCE 1998;124:892–900.
[45] Lemaitre J. A continuous damage mechanics model for ductile fracture. J Engng Mater Technol 1985;107:83–9.
[46] Lemaitre J, Chaboche J-L. Mechanics of solid materials. London: Cambridge University Press; 1990.
[47] Lemaitre J. A short course in damage mechanics. New York: Springer-Verlag; 1992.
[48] Loland KE. Continuous damage model for load-response estimation of concrete. Cem Concr Res 1980;10:395–402.
[49] Lubarda VA, Kracjinvovic D, Mastilovic S. Damage model for brittle elastic solids with unequal tensile and compressive strength. Engng Fract Mech 1994;49:681–97.
[50] Lubliner J, Oliver J, Oller S, Onate E. A plastic-damage model for concrete. Int J Solids Struct 1989;25:299–326.
[51] Mazars J, Pijaudier-Cabot G. Continuum damage theory – application to concrete. J Engng Mech 1989;115:345–65.
[52] Menetrey Ph, Willam KJ. Triaxial failure criterion for concrete and its generalization. ACI Struct J 1995;92:311–8.
[53] Meschke G, Lackner R, Mang HA. An anisotropic elastoplastic-damage model for plain concrete. Int J Numer Methods Engng 1998;42:703–27.
[54] Murakami S, Ohno N. A continuum theory of creep and creep damage. In: Proceedings third IUTAM symposium on creep in structures. Berlin: Springer; 1981. p. 422–44.
[55] Nguyen GD. A thermodynamic approach to non-local damage modeling of concrete. Int J Solids Struct 2008;45:1918–34.
[56] Nooru-Mohamed MB. Mixed-mode fracture of concrete: an experimental approach. Ph.D. Dissertation. Delft, The Netherlands: Delft University of Technology; 1992.
[57] Ohtani Y, Chen WF. Multiple hardening plasticity for concrete materials. J Engng Mech ASCE 1988;114:1890–910.
[58] Onate E, Oliver S, Lubliner J. A constitutive model of concrete based on the incremental theory of plasticity. Engng Comput 1988;5:309–19.
[59] Ortiz M. A constitutive theory for the inelastic behavior of concrete. Mech Mater 1985;4:67–93.
[60] Ortiz M, Popov EP. Plain concrete as a composite material. Mech Material 1982;1:139–50.
[61] Ortiz M, Pandolfi A. Finite-deformation irreversible cohesive elements for three-dimensional crack-propagation analysis. Int J Numer Methods Engng 1999;44:1267–82.
[62] Pijaudier-Cabot G, Bazant ZP. Nonlocal damage theory. ASCE J Engng Mech 1987;113:1512–33.
[63] Rabotnov YUN. Creep rupture. In: Proceedings of the XII international congress on applied mechanics. Stanford-Springer; 1968. p. 342–9.
[64] Resende L, Martin JB. A progressive damage continuum model for granular materials. Comput Methods Appl Mech Engng 1984;42:1–18.
[65] Salari MR, Saeb S, Willam KJ, Patchet SJ, Carrasco RC. A coupled elastoplastic damage model for geomaterials. Comput Methods Appl Mech Engng 2004;193:2625–43.
[66] Schreyer HL. Third-invariant plasticity theory for frictional materials. J Struct Mech 1983;11:177–96.
[67] Simo JC, Honein T. Variational formulation, discrete conservation laws, and path domain independent integrals for elasto-viscoplasticity. J Appl Mech Trans ASME 1990;57:488–97.
[68] Simo JC, Hughes TJR. Computational inelasticity: interdisciplinary applied mathematics. New York: Springer; 1998.
[69] Simo JC, Ju JW. Strain and stress-based continuum damage model. Part I: formulation. Int J Solids Struct 1987;23:821–40.
[70] Simo JC, Ju JW. Strain- and stress-based continuum damage models. Part II: computational aspects. Int J Solids Struct 1987;23:841–69.
[71] Sinha BP, Gerstle KH, Tulin LG. Stress–strain relations for concrete under cyclic loading. ACI J Proc 1964;61:195–212.
[72] Taylor RL. FEAP: a finite element analysis program for engineering workstation. Rep. No. UCB/SEMM-92 (Draft version). Berkeley: Department of Civil Engineering, University of California; 1992.
[73] Voyiadjis GZ, Abu Al-Rub RK. A finite strain plastic-damage model for high velocity impacts using combined viscosity and gradient localization limiters, Part II: numerical aspects and simulation. Int J Damage Mech 2006;15:335–73.
[74] Voyiadjis GZ, Abu-Lebdeh TM. Plasticity model for concrete using the bounding surface concept. Int J Plasticity 1994;10:1–21.
[75] Voyiadjis GZ, Park T. Anisotropic damage effect tensors for the symmetrization of the effective stress tensor. J Appl Mech ASME 1997;64:106–10.
[76] Voyiadjis GZ, Kattan PI. Advances in damage mechanics: metals and metals matrix composites. Oxford: Elsevier; 1999.
[77] Voyiadjis GZ, Abu Al-Rub RK, Palazotto AN. Non-local coupling of viscoplasticity and anisotropic viscodamage for impact problems using the gradient theory. Arch Mech 2003;55:39–89.
[78] Voyiadjis GZ, Abu Al-Rub RK, Palazotto AN. Thermodynamic framework for coupling of non-local viscoplasticity and non-local anisotropic viscodamage for dynamic localization problems using gradient theory. Int J Plasticity 2004;20:981–1038.
[79] Voyiadjis GZ, Taqieddin ZN, Kattan PI. Anisotropic damage-plasticity model for concrete. Int J Plasticity 2008;24:1946–65.
[80] William KJ, Warnke EP. Constitutive model for the triaxial behavior of concrete. In: International association of bridge and structural engineers, seminar on concrete structure subjected to triaxial stresses, Paper III-1, Bergamo, Italy, May 1974, IABSE Proc. 19; 1975.
[81] Wu JU, Li J, Faria R. An energy release rate-based plastic-damage model for concrete. Int J Solids Struct 2006;43:583–612.
[82] Yazdani S, Schreyer HL. Combined plasticity and damage mechanics model for plain concrete. J Engng Mech (ASCE) 1990;116:1435–50.
[83] Zhang QY. Research on the stochastic damage constitutive of concrete material. Ph.D. Dissertation. Shanghai, China: Tongji University; 2001.